2013

Implementation And Model To Model Intercomparison Of 12 Heat Stress Metrics

Jonathan Robert Buzan
Purdue University, jrbuzan@gmail.com

Graduate School ETD Form 9
(Revised 12/07)

PURDUE UNIVERSITY
GRADUATE SCHOOL
Thesis/Dissertation Acceptance

This is to certify that the thesis/dissertation prepared

By Jonathan Robert Buzan

Entitled

IMPLEMENTATION AND MODEL TO MODEL INTERCOMPARISON OF 12 HEAT STRESS METRICS

For the degree of Master of Science

Is approved by the final examining committee:

Ernie Agee
Chair

Matthew Huber

H. Jay Melosh

To the best of my knowledge and as understood by the student in the *Research Integrity and Copyright Disclaimer (Graduate School Form 20)*, this thesis/dissertation adheres to the provisions of Purdue University's "Policy on Integrity in Research" and the use of copyrighted material.

Approved by Major Professor(s): Ernie Agee

Approved by: Indrajeet Chaubey 11/25/2013
Head of the Graduate Program Date

IMPLEMENTATION AND MODEL TO MODEL INTERCOMPARISON OF 12 HEAT STRESS METRICS

A Thesis

Submitted to the Faculty

of

Purdue University

by

Jonathan R. Buzan

In Partial Fulfillment of the

Requirements for the Degree

of

Master of Science

December 2013

Purdue University

West Lafayette, Indiana

ACKNOWLEDGEMENTS

Jonathan R. Buzan thanks the members of his committee—Jay Melosh, Ernie Agee, and Matthew Huber—for their time, effort, and patience. He also thanks Rachel Gipe for her work and friendship. The members of the Climate Dynamics Prediction Laboratory, Aaron Goldner, Nicholas Herold, and Paul Acosta have supported Jonathan through thick and thin. Jonathan thank sKeith Oleson for his dedication to the project. Lastly, Jonathan thanks Jacob Carley for his help with programming resources and inciteful comments.

TABLE OF CONTENTS

Page

LIST OF TABLES

LIST OF FIGURES

Figure Page

Figure Page

ABSTRACT

Buzan, Jonathan R. M.S., Purdue University, December 2013. Implementation and Model to Model Intercomparison of 12 Heat Stress Metrics. Major Professor: Matthew Huber.

Earth system models simulate the dynamics of the most complex systems on our planet with some success. Despite the overwhelming sophistication of these models, which include dynamical interactions of ocean, atmosphere, vegetation, ice, and land-surface properties, they fail to include the most important element. People. Humans are also a complex physical-biological system and coupling of human physiology within an Earth Systems Modeling framework is challenging. This thesis presents results that tackle one particular component of human physiological climate interaction—a representation of heat stress on human physiology. Twelve different metrics were implemented and analyzed. These metrics represent a variety of philosophical approaches to characterizing heat stress: thermal comfort, physiological responses, and first principle physics. We implemented these 12 metrics into the Community Land Model (CLM4.5). All of the metrics implemented measure the covariance of near surface atmospheric variables: temperature, pressure, and humidity. Results show that heat stress may be broken into two regimes; arid and non-arid regions (i.e. the rest of

the land surface). Additionally, results show that the highest heat stress zones are a robust feature with low variability. Temperatures vary by ±3°C as compared to ±1°C wet bulb temperatures, and is consistent over a vast area of Earth.

1. INTRODUCTION

Heat stress occurs when the human body loses the ability to internally regulate heat balance, and an increase of internal temperatures of ~3°C can be lethal. Many different heat diagnostic indices have been developed to diagnose heat stress, and policy makers have made decisions to incorporate these indices in weather warning systems. Heat warnings have been targeted to reduce morbidity due to heat stroke and heat exhaustion. Despite the implementation of warning systems, such as national notices and work guidelines for hot environments, heat death remains the number one cause of death from natural disaster in First World countries; more than tornados, flooding, and hurricanes combined. The 2010 heat wave in Russia is the worst recorded heat wave, with 50,000 deaths.

Heat waves can be defined by heat indices, such as the Wet Bulb Globe Temperature (*WBGT*), the Discomfort Index (*DI*), or Heat Index (*HI*). Heat indices were developed to reduce morbidity and mortality by directing the creation of policies to minimize risk. None of these metrics are coupled to weather forecast models on short time scales, nor better decision making on longer time scales with Earth system models. Furthermore, indices, such as *HI* or *WBGT*, do not account for complex physiology.

Prognostic physiological heat stress models consider wind, ambient temperature, and moisture from the environment, as well as internal processes, such as blood flow and sweat that help regulate internal temperatures. There are numerous different forms of prognostic physiological models. Some of them are quite complicated, using hundreds of grid cells to represent all parts of the body. Unfortunately, these models are computationally expensive. Less complicated models represent the human body as a single cylinder with multiple layers. Unfortunately, neither computational method is coupled to Earth system models.

Simple diagnostic physiological models are coupled to climate models, and, at best, are reliant on climatological data sets. These datasets range in complexity; from atmospheric variables such as temperature, pressure and humidity, to even having solar and thermal radiation. The datasets are either an observational gridded format, but often these datasets are reanalysis products. A reanalysis product is an Earth system model forced with an observational dataset to generate the state of atmosphere. We use a combination of Earth system models, reanalysis, and observational data products to analyze heat stress.

Using the Community Land Model (CLM4.5) of the Community Earth System Model (CESM1.2) developed by the National Center for Atmospheric Research (NCAR), we implement 12 different metrics. These heat stress metrics cover three philosophical approaches—comfort, physiology, and empirically based algorithms. Comfort based routines rationalize what animals and humans feel. Algorithms based upon physiology rationalize responses such as heart rate and core temperatures. Empirically based

algorithms use comparisons to worker productivity or theoretical first principle physics. The algorithms all use temperature, humidity, and pressure—atmospheric variables—in their calculation. Additionally, with the importance of moisture in these calculations, the heat stress metrics are built upon a foundation of the using the most improved water thermodynamic calculations available. We implemented new water vapor calculations. The advantage of adding these metrics within the climate model framework are two-fold: 1) improve the thermodynamic calculations within climate models, and 2) to quantify the modern state of human/mammalian heat stress.

Our results show systematic differences between the comfort and empirically based algorithms. Algorithms based on purely thermodynamic states (not heat load), show low latitudes (±20°) have a nearly constant state of heat stress throughout a year. Mid-latitudes (±30-45°) show that heat stress has a large regional dependency on 'heat load', and not just thermodynamic state. Arid regions have large evaporative cooling potential, but also have large sensible heat load. The areas that have the highest heat stress in the world also correspond to the regions with highest convective potential, i.e. monsoons.

2. BACKGROUND

2.1 What is Heat Stress

Heat balance is modulated by many different mechanisms within the human/environment system, a process known as homeostasis. Heat stress occurs when the human body loses the ability to internally regulate heat balance. In hot environments the breakdown in homeostasis causes hyperthermia. Losing homeostasis induces rapid increase in core body temperatures, and an increase of internal temperatures of ~3°C can be lethal (Simon, 1993). For example, heat is generated within the core body depending on levels of activity; from a minimum at rest up to ~8x the rest state due to strenuous activity. While these activities increase heat production within the human body, to maintain homeostasis, blood flow transfers this heat to the skin. At the skin, heat transfer is dependent on the environment. There are four different methods of heat transport at the exterior of a human body: radiation, convection, conduction, and evaporation (Simon, 1993; Koppe et al., 2004; Gaughan et al., 2009). As temperatures increase outside the human body (hot environment), the primary method of removing excess heat is through evaporation; controlling ~75% of heat loss (Koppe et al., 2004). Future climate scenarios show that conditions become too humid, the human body will no longer be able to use sweat to remove heat, and

cannot survive without air conditioning over large parts of the Earth (Sherwood and Huber, 2010).

2.2 Human Thermoregulatory Mechanisms

Humans have a variety of systems that interact to cope with heat stress in order to maintain homeostasis. Hyperthermia occurs when the body is overwhelmed by internal heat production (Simon, 1993). The hypothalamus, a portion of the brain responsible for the autonomic (peripheral) nervous system, regulates thermal control. The hypothalamus senses core body temperatures and releases (or shuts off) chemical compounds to induce a variety of organs to react. For example, the hypothalamus may induce a fever, forcibly raise internal temperatures releasing certain enzymes, which increase metabolic production. In normal thermoregulation, as internal temperatures rise the hypothalamus initiates vasodilation (dilation of the blood vessels) (Simon, 1993), and also increases heart rate (Yokota et al., 2008). This promotes internal heat transport to the skin. Sweat removes heat through evaporation. The numerous glands in human skin produce both sweat and sebum (fatty secretions), and the sebum acts as emulsifier to prevent sweat from dripping off the skin, enhancing the capability of reaching maximum heat loss by evaporation (Lupi, 2008). However, if the local moisture conditions in the environment reduce the effectiveness of evaporation, the hypothalamus will not be able to regulate heat. At extreme temperature and moisture conditions, thermoregulation is impossible.

The human body has the capacity to adapt to a variety of environments through acclimatization. Respiration rates, oxygen volume, and gas exchanges are heavily dependent on whether subjects are acclimatized or not (Pandolf and Kamon, 1974). Physical fitness (Gardner et al., 1996), and age, all factor into the body's ability to deal with heat stress. For example, fatty tissues have about half the thermal conductivity of other tissues. The percentage and distribution of fat will have an impact on thermal stress. A physically fit individual can produce up to 3 liters of sweat per hour (Koppe et al., 2004), maximizing evaporative potential cooling mechanisms. The heart blood pressure and flow rates will increase or reduce depending on the environment, adjusting heat transfer to the skin. Additionally, the human vascular system reacts to prolonged strenuous exposure (Koppe et al., 2004). If the local temperatures increase, the human body will react by increasing the density of blood vessels in the skin. Likewise, as temperatures fall, the body will reduce the density of blood vessels in the skin. Additionally, humans adapt to altitude changes by changing the density of air sacs within the lungs, changing the evaporative potential in the lungs, as well as maintain high blood oxygen content.

2.3 Heat Stress Links between Animals and Humans

Endothermic (warm-blooded) animals thermally regulate their internal temperatures, and are often used as an analogue to the human body in heat stress studies (Bynum et al., 1978; Hightower and Guidon, 1989). Animal physiology deals with heat stress in many complicated ways. Horses and cattle die when core

temperatures reach ~43°C for up to two hours (Gaughan et al., 2009), as do humans (Simon, 1993). Cattle temperatures follow sun radiation, but lag ~2 hours when in the shade, and their reaction becomes more complicated as strenuous exposure occurs over 3-4 days (Gaughan et al., 2009). In some large ungulates (hoofed mammals), there are specialized blood vessels (cartotid retes) that run near the evaporative cooling areas in the head before entering the brain, however, this process shuts down when in 'fight or flight' excessive exercise (Mitchell et al., 2002). Baboons live in strenuous hot environments and can survive increased exposure to solar radiation, provided they have adequate access to water (Mitchell et al., 2009). However, even baboons have complex inflammatory responses when they suffer heat stroke (Bouchama et al., 2005). Such inflammatory responses, like cytokines signaling molecules, effect baboons in similar ways to human responses for heat stress (Mitchell et al., 2009). Smaller animals (e.g. squirrels) will seek underground shelter when their internal temperatures rise (Gaughan et al., 2009), and the quasi-poikilothermic (cold-blooded) naked mole rat regulates its temperatures through huddling and controlled underground environments (Withers and Jarvis, 1980; Buffenstein and Yahav, 1991). Marsupials approach heat stress through a different mechanism; a 30% less active metabolism rate when compared to their eutherian counterparts (Dawson and Hulbert, 1970). The data sets derived from these previously executed experiments on animals are used to compare and drive heat stress models.

2.4 Heat Stress Modeling

2.4.1 Diagnostic Models

The models for determining heat stress for the human body vary; ranging from simple indices to complex prognostic physiology modeling. Heat Index (*HI*) is a polynomial equation used by the National Weather Service (NWS) for measuring apparent temperature ('feels like' temperature). The equation is used to determine when to issue heat warnings (Steadman, 1979; Rothfusz, 1990). *HI* was calibrated for working conditions, and work to rest ratios were developed for labor policies towards heat stress.

The Wet Bulb Globe Temperature (*WBGT*) is an empirical diagnostic index developed for the United States military as a warning system to prevent heat stress casualties (Minard et al., 1957; Cain, 2006). The diagnostic uses a combination of dry bulb temperature, wet bulb temperature (the temperature a parcel cools to when water is evaporated until saturation), and the globe thermometer (a measure of both advective and radiation temperatures). There are numerous simplifications of *WBGT* geared towards avoiding using iterative methods of complex calculations for both wet bulb and globe thermometers. Some methods use 'indoor' *WBGT*, and calculation assumes that the radiation temperature of the globe thermometer to be equal to the dry bulb temperature, and merges the two quantities (Hyatt et al., 2010). Another widely used adaptation is the Simplified *WBGT* (*sWBGT*). The *sWBGT* equation does away with the wet bulb and globe thermometers entirely, and uses a combination of dry

bulb temperature and vapor pressure (Fischer et al., 2012; Kjellstrom et al., 2009; Willett and Sherwood, 2010).

The before mentioned methods have been criticized for oversimplification and inaccuracies (Budd, 2008). The Australian Bureau of Meteorology acknowledges that *sWBGT* should always assume the subject is in the shade (ABOM, 2010). The numerous calculations of the simplifications of wet bulb temperature may also add errors to the calculations (Alfano et al., 2012), and the sources for these calculations have been attributed to the wrong authors (Budd, 2008). Advanced calculations for wet bulb and globe thermometers have been developed for the highest accuracy (Davies-Jones, 2008; Liljegren et al., 2008; Azer and Hsu, 1977). We discuss wet bulb temperature calculations in detail in section 2.6, because multiple diagnostics use wet bulb temperature, such as the Discomfort Index.

Discomfort Index (*DI*) uses a combination of wet bulb and dry bulb temperatures and has been in use for more than 4 decades, like the *WBGT*. *DI* is used by the Israel Defense Forces for hot and humid or dry climates (Epstein and Moran, 2006). The *DI* was originally developed to address issues with 'cooling degree days' (Thom, 1959). Cooling degree days are a measurement of the qualitative amount of air conditioning required to cool a household to a comfortable value. To calculate the value required averaging the high and low temperatures and compare them to a baseline. There were two problems with cooling degree days. The first was a lack of standardization between companies (the baseline values were not the same). Second, the amount of moisture in the air was not considered in cooling degree days. This may have a substantial impact

on air conditioning costs. The *DI* was developed to address both of these issues by setting up a standardized baseline and moisture calculations for cooling degree days.

Humidex (*HUMIDEX*) uses a combination of dry bulb temperature and vapor pressure to quantify human discomfort in excessive heat and humidity for the average person (Masterson and Richardson, 1979). The index was developed in Canada, and is used by both Canada and European countries (Barnett et al., 2010; CCOHS, 2013). *HUMIDEX* has been used in recent studies regarding heat stress and heat stress mortality (Conti et al., 2005; Oleson et al., 2013; Vaneckova et al., 2011). These studies largely focus on city to city comparisons, whether through model or through datasets to combine meteorology and biology.

Universal Thermal Climate Index (*UTCI*) was developed to determine human heat stress through biometeorology (Bröde et al., 2011; Fiala et al., 2011; Havenith et al., 2011), with the intention of integration into weather prediction models (Jendritzky et al., 2010). The effort failed to couple the prognostic thermal model of humans into the Earth system model framework, however, the *UTCI* was the resulting product. One of the major criticisms of major heat stress metrics is the lack of wind and radiation parameterizations. The *UTCI* includes parameterizations of wind and radiation. The index is a polynomial fit to ensemble simulations of weather effects on humans with coefficients being dry bulb, wet bulb, and radiation temperatures.

There are many guidelines for working conditions in hot environments. The Occupational Safety and Health Administration (OSHA) ensured strict heat stress safety measures in response to the British Petroleum (BP) gulf oil spill (OSHA.gov, 2010). OSHA

required frequent breaks, working at cooler times of the day, and multiple other directives. The International Organization for Standardization (ISO) has policies for measuring heat stress and determining workload within the workplace. ISO 7243 uses the *WBGT* as the standard (Parsons, 2006). The original *WBGT* assumed the worker was wearing light trousers and olive drab t-shirts (US Marine Corps training clothing) (Minard et al., 1957). ISO 7243 introduces a modification to account for different clothing types by setting the estimated metabolic work rate higher to account for the clothing.

Numerous studies have evaluated potential changes in worker capacity in a global change perspective (Nilsson and Kjellstrom, 2010; Hyatt et al., 2010; Baker et al., 2002; Kjellstrom et al., 2008; Kjellstrom et al., 2009). However, very few studies have used the direct environment in global climate modeling as a method of quantifying future impacts, and those that have, used simplified indexes (Fischer and Knutti, 2012; Fischer et al., 2012; Dunne et al., 2013). These studies are discussed in further detail in section 2.8.

2.4.2 Prognostic Models

The human body is a complex system, and prognostic physiology models reflect this. A basic physiology model assumes the human body is a series of layers from the core to the skin (Khan et al., 2004). Complicated models build upon this assumption by representing the body as a series of compartments within geometric shapes (Kraning and Gonzalez, 1997), and add further complexity by dividing the body into multiple segments (Fiala et al., 1999; Fiala et al., 2001). Fiala et al. (2001) attempted to couple

their model into weather forecasting models. Unfortunately, due computational cost, the project was not feasible to couple to weather models. Instead, the model was run with a series of initial conditions and average weather output was used for the development of the *UTCI* (Jendritzky et al., 2010).

SCENARIO is a physiology heat stress model designed for athletic, industrial, and military thermal stress applications (Kraning and Gonzalez, 1991; Kraning and Gonzalez, 1997; Gonzalez, 2004). Additionally, SCENARIO is a simplification of an astronaut thermal model developed by NASA (Stolwijk, 1971). The model use a series of six first principle differential equations and boundary conditions to solve for heat transport from the core to the skin of the human body, resulting in a prognostic value for body temperature. Components involve blood flow, oxygen intake rate, heart rate, sweating, etc., which are all dynamic properties of the model. Boundary conditions include clothing and environmental conditions and metabolic energy production. The model is verified by data sets from controlled experiments and is used by the United States Army Research Institute of Environmental Medicine (USARIEM) to test a variety of experimental clothing and environmental conditions (Santee and Matthew, 2000; O'Brien et al., 2008). SCENARIO has also been verified by heat stress experiments using internal temperature sensors (Byrne et al., 2006; Buller et al., 2010). Furthermore, SCENARIO is one of the few prognostic models that has been used for both men and women (Gonzalez et al., 2010; Yokota et al., 2011; Yokota et al., 2012). USARIEM currently uses SCENARIO to predict heat stress for the full range of military clothing and climates (personal communication, R. Gonzalez).

2.5 The Structure of Climate Models

There are a variety of different Earth systems models used for research, and one such model is the National Center for Atmospheric Research (NCAR) Community Earth System Model version 1 (CESM1, hence CESM). CESM is one of the models that is used in the Intergovernmental Panel on Climate Change (IPCC), the purpose of which is to compile and assess climate research. The IPCC guides climate modeling research by enabling the experimental framework used to compare all the major climate models, called the Climate Model Inter-comparison Project 5 (CMIP5). CMIP5 has 5 major types of modeling experiments: evaluation (1850-2005), projection (Representative Concentration Pathways, RCP), climate sensitivity and feedbacks, carbon cycle, and clouds (Taylor et al., 2012). All participating models must run these experiments for comparison to each other.

CESM is made of component models: Community Atmosphere Model version 4/5 (CAM4 and CAM5), Parallel Ocean Program (POP), Community Sea Ice Model (CSIM), and the Community Land Model version 4.5 (CLM4.5, hence CLM). CLM is the target model for implementing the physiological component of our research, and has received a new update. Within CLM are topography, dynamic vegetation, land-air interaction, and urban environments. Built within CLM is a carbon-nitrogen cycle model that produces prognostic values for vegetation and soil (Lawrence et al., 2011; Lawrence et al., 2012; Oleson et al., 2013). Vegetation is discretized into 15 plant functional types (PFT), that can coexist with up to three other PFTs in the same model grid cell (constituting a 'biome'), consistent with ecological theory (Bonan et al. 2002). These

biomes range from broadleaf evergreen trees to tundras. Additionally, the river transport model has been upgraded to include a variation on the Variable Infiltration Capacity (VIC) Macroscale Hyrdrologic Model (Oleson et al., 2013). There are new parameterizations and models for snow cover, lakes, crops, and urban classifications (Oleson et al., 2013). The urban biome, a specialized canyon model, is designed to represent the 'heat island' where temperatures are amplified by urban environments (Oleson et al., 2008a,b; Oleson et al., 2010a,b). The 'heat island' effect can increase the likelihood of complications from human heat stress. Radiation is 'trapped' within the walls of the 'canyon', and air conditioners add waste heat to the local environment. Past CLM4 experiments have explored and contrasted heat between the rural and urban environments (Oleson et al., 2011), and found an average increase of ~3°C in the urban areas. Future scenarios show at higher CO_2 concentrations that urban environments have temperature increases of ~4°C (Oleson, 2012).

2.6 Thermodynamic Water Calculations

Humans dissipate ~75% of their heat through the evaporation of sweat from the skin of the human body. Therefore, incorporating detailed and accurate calculations of water vapor in the atmosphere of is a critical step for the understanding global heat stress. Specifically, the potential to cool from evaporation is particularly of interest, and is measured from a quantity called wet bulb temperature. Wet bulb temperatures measure the temperature a parcel of air will cool to from the evaporation of water into that parcel until reaching parcel saturation. The wet bulb temperature calculations

created by Davies-Jones (2008) are the most detailed, computationally fast, and accurate of its kind. The Davies-Jones (2008) calculation improves upon theory and previous calculation techniques (Bolton, 1980). Davies-Jones (2008) shows that the the second order derivative of the equivalent potential temperature function, with respect to the wet bulb temperature and pressure, is a linear function from an interval of -20°C–20°C over a expansive pressure range of the entire atmosphere. Using quadratic expressions, these derivatives are used to calculate an extremely accurate 'first guess' requiring only 1 or 2 iterations using the Newton-Raphson method. The Davies-Jones (2008) calculation is both accurate and computationally faster than Bolton's (1980) previous work.

We must introduce some terminology to describe the Davies-Jones (2008) calculation. All temperature subscripts that are capitalized are in Kelvin, while lower case are in Celsius. κ_d is the Poisson constant for dry air, and λ is the inverse. It is useful to scale many of the following equations using non-dimensional pressure, π:

$$\pi = (p/p_0)^{1/\lambda} \tag{2.1}$$

where p is the pressure, and p_0 is a reference pressure (1000mb).

To define wet bulb temperature, T_w, we must determine the equivalent potential temperature, Θ_E. Determining Θ_E is a three step process:

$$T_L = \frac{1.}{\frac{1.}{T-55.} - \frac{\ln(RH/100.)}{2840.}} + 55. \tag{2.2}$$

where T is the parcel temperature (Kelvin) and RH is the relative humidity (%). The lifting condensation temperature, T_L, calculated from equation 22 Bolton (1980), is the

temperature point that a parcel that is lifted, following a dry adiabatic lapse rate, begins to condense. As the air rises further, the parcel now follows a moist potential temperature, Θ_{DL}:

$$\theta_{DL} = T * \left(\frac{p_0}{p-e}\right)^{\kappa_d} \left(\frac{T}{T_L}\right)^{(r*0.00028)} \tag{2.3}$$

where *e* is the parcel vapor pressure (mb), and *r* is the mixing ratio (g/kg). At this point in the calculation, the parcel is raised to a great height where all latent heat is transferred to the air parcel, and the water is rained out, giving the solution to Θ_E. There are many forms of calculating this process. The analytical solution (Holton, 1972) is computationally prohibitive in atmospheric models. There are various approximations of different aspects of potential and saturated temperatures to calculate Θ_E (Betts and Dugan, 1973; Simpson, 1978), however, many of them are with large errors. These errors are compared in Bolton (1980), and equation 39 (Bolton's formulation) is up to an order of magnitude more accurate than previous formulations.

$$\theta_E = \theta_{DL} * \exp\left[\left(\frac{3.036}{T_L} - 0.001788\right) r(1. + 0.000448r)\right] \tag{2.4}$$

Equivalent temperature, T_E, is the equivalent potential temperature scaled by non-dimensional pressure:

$$T_E = \theta_E \pi \tag{2.5}$$

The initial guess for T_w is based upon regions where the second order derivative of equivalent potential temperature reaches a linear relationship with variations in T_w and λ. Two coefficients are derived (Davies-Jones, 2008):

$$k1 = -38.5\pi^2 + 137.81\pi - 53.737 \tag{2.6}$$

$$k2 = -4.392\pi^2 + 56.831\pi - 0.384 \tag{2.7}$$

The evaluation of errors at a variety of pressures necessitated that Davies-Jones develop a regression line on colder regions of the initial guess:

$$D = \left(0.1859\frac{p}{p_0} + 0.6512\right)^{-1} \tag{2.8}$$

where *D* is used for calculating transition points between quadratic fits to the second order derivatives of the equivalent potential temperature. The initial guess of T_w for coldest temperatures is (Davies-Jones, 2008 equation 4.8):

$$T_w = T_E - C - \frac{Ar_s(T_E, \pi)}{1. + Ar_s(T_E, \pi)\frac{\partial \ln(e_s)}{\partial T_E}} : (C/T_E)^\lambda > D(\pi) \tag{2.9}$$

where *A* is constant, and r_s is saturated mixing ratio. T_w for all other temperature regimes is governed by equations 2.10-12 (Davies-Jones, 2008 equations 4.9-4.11):

$$T_w = k1(\pi) - 1.21 * cold - 1.45 * hot - (k2(\pi) - 1.21 * cold) * (C/T_E)^\lambda + (0.58/(C/T_E)^\lambda) * hot \tag{2.10}$$

$$cold = \begin{cases} = 0 : 1 \leq (C/T_E)^\lambda \leq D(\pi) \\ = 1 \end{cases} \tag{2.11}$$

$$hot = \begin{cases} = 1 : T_E > 355.15 \\ = 0 \end{cases} \tag{2.12}$$

where the combination of equations' initial guesses are valid from 1050mb to 100mb. Following the initial guess, up to two iterations using the Newton-Raphson method are required to reach the 'true' wet bulb temperature. An August-Roche-Magnus

formulation of the Clausius-Clayperon equation (Bolton, 1980; Lawrence, 2005) is used for determining the saturation vapor pressure at T_W:

$$e_s = 6.112 \exp\left(\frac{a(T_W - C)}{T_W - C + b}\right) \tag{2.13}$$

where e_s is in mb, a and b are constants, while C is the temperature of freezing at standard pressure. This equation determines the saturated mixing ratio, r_s:

$$r_s(T_W) = \frac{\varepsilon e_s(T_W)}{(p_0 \pi^\lambda - e_s(T_W))} \tag{2.14}$$

Following Davies-Jones, we use the derivative of the August-Roche-Magnus equation for calculating the derivative of the saturated mixing ratio, equations 2.15-2.17.

$$\frac{\partial \ln(e_s)}{\partial T_W} = \frac{ab}{(T_W - C + b)^2} \tag{2.15}$$

$$\frac{\partial e_s}{\partial T_W} = e_s \frac{\partial \ln(e_s)}{\partial T_W} \tag{2.16}$$

$$\left(\frac{\partial r_s}{\partial T_W}\right)_\pi = \frac{\varepsilon p}{(p - e_s(T_W))^2} \frac{\partial e_s}{\partial T_W} \tag{2.17}$$

Now, we return to equivalent potential temperature, and substitute T_L for T_W:

$$f(T_W; \pi)) = \left(\frac{C}{T_W}\right)^\lambda \left[1. - \frac{e_s}{p_0 \pi^\lambda}\right]^{\nu\lambda} \exp(-\lambda G(T_W; \pi)) \tag{2.18}$$

where:

$$G(T_W, \pi) = \left(\frac{3036.}{T_W} - 1.78\right) [r_s(T_W, \pi) + 0.448 * r_s^2(T_W, \pi)] \tag{2.19}$$

The derivative of the function 2.18 is required for the Newton-Raphson method:

$$f'(T_W;\pi)) = -\lambda\left[\frac{1.}{T_W} + \frac{\nu}{(p-e_s)}\frac{\partial e_s}{\partial T_W} + \left(\frac{\partial G}{\partial T_W}\right)_\pi\right] \quad (2.20)$$

where the derivative of $G(T_W, \pi)$:

$$\left(\frac{\partial G}{\partial T_W}\right)_\pi = -\frac{3036.*(r_s+0.448r_s^2)}{(T_W^2)} + \left(\frac{3036.}{T_W} - 1.78\right)(1.+2.*0.448r_s)\left(\frac{\partial r_s}{\partial T_W}\right)_\pi \quad (2.21)$$

and, due to the linear relationship of the second order derivative of equation 2.18, we may accelerate the Newton-Raphson method using the initially calculated T_W and T_E.

$$T_w = T_w - \frac{f(T_W;\pi) - \left(\frac{C}{T_E}\right)^\lambda}{f'(T_W;\pi)} \quad (2.22)$$

Normally, the Newton-Raphson method is inefficient; the function requires massive amounts of computational power to reach a solution. The accuracy of the first guess allows the Newton-Raphson method to be iterated once or twice before converging. Thus, this process is efficient and accurate. The calculation of the wet bulb temperature, saturated vapor pressure, and relative humidity are restricted by the accuracy initial inputs. Normally, in CLM, these inputs are calculated from the polynomial fits to the Clausius-Clayperon theory (Wexler, 1976; Wexler, 1977; Flatau et al., 1992). The method described above is valid over a larger range of pressures as the polynomial fits only give unrealistic values at pressures below 300 mb. Additionally, the accurate calculation T_w is imperative for many metrics that are used for determining heat stress.

2.7 Heat Stress Calculations

Heat Index (*HI*), Discomfort Index (*DI*), Apparent Temperature (*AT*), Simplified *WBGT* (*sWBGT*), and Humidex (*HUMIDEX*) all share common characteristics. Each index uses a combination of atmospheric variables: temperature, humidity, and pressure. *HI* and *AT* are based upon deviations from a comfort zone based upon changes in moisture and humidity from human thermal modeling (Steadman, 1979). *sWBGT* (Willett and Sherwood, 2010) is a simplified version of the complicated index *WBGT*, which is an empirically derived index (Minard et al., 1957). The different atmospheric variables are weighted dependent upon assumptions (such as local climate or the 'average' human) and the experimental design that was used to create these indexes; factors such as local climate, or the 'average' human. Complicated heat indices include components beyond the basic atmospheric state variables, such as radiation transfer and winds, accounting for convective and radiative energy fluxes.

The primary focus of this work is on the atmospheric variable based metrics, not fluxes. The atmospheric variables involved in these metrics are in various forms. Some require vapour pressure, others require relative humidity. A common calculation for vapor pressure:

$$e_{RH} = (RH/100.) * e_{sPa} \tag{2.23}$$

involves the *RH* and the saturated vapor pressure (e_{sPa}), in Pascals. Otherwise, metrics will use either Kelvin or Centigrade and Pascals or millibars. Some of the more advanced atmospheric variable metrics will include a function for wind (Steadman, 1994). Note

that most of these metrics are displayed as a temperature. The metrics have temperature scales for comparative purposes only, as the metrics are a measure of heat load, not temperature. We will break these metrics into a variety of sub-categories, based upon their design philosophies: comfort, physiological response, and empirical fit.

2.7.1 Comfort Algorithms

The underlying philosophical approach to deriving comfort metrics is representing behavioral reactions to levels of comfort (Masterson and Richardson, 1979; Steadman, 1979). The goal of these rationalized equations of comfort is to match the levels of discomfort to issue warnings for laborers (Gagge et al., 1972) and livestock (Renaudeau et al., 2012). Discomfort in humans sets in much earlier than actual physiological responses, i.e. the human body provides an early warning to the mind that continuing the activity will lead to disastrous consequences. For example, when heat exhaustion sets in, the body is sweating profusely, and often there are symptoms of dizziness. However, the actual core temperature is defined for heat exhaustion is at 38.5°C, which is considerably lower than heat stroke (42°C). *AT*, *HI*, *HUMIDEX*, and Temperature Humidity Index (*THI*) account for the comfort level, and they have been tailored to the region they were developed in or have been streamlined for ease of use.

Apparent Temperature was developed using a combination of wind, radiation and heat transfer to measure thermal comfort and thermal responses in humans (Steadman, 1994). *AT* was developed for the Australian Bureau of Meteorology, and the

climates of Australia. The metric is an approximation of a thermal model of human comfort (Steadman 1979a,b; Steadman, 1984), and is as follows:

$$AT = T_c + \frac{3.30e_{RH}}{1000.} - 0.70 * u_{10m} - 4.0 \quad (2.24)$$

where u_{10m} (m/s) is the wind velocity measured at 10m, and *AT* is in degrees Celsius. Of the metrics we are describing, this is the only metric that includes wind velocity in its equation; the others have the wind velocity in their assumptions. An assumption for *AT* is that the subject is outside, but not exposed to direct sunlight.

Heat Index (*HI*) was developed using a similar process as *AT*. The United Stated National Weather Service (NWS) required a heat stress early warning system, and the index is a polynomial fit to Steadman's (1979a) comfort model.

$$HI = -42.379 + 2.04901523T_f + 10.14333127RH + -0.22475541T_fRH + -6.83783\times10^{-3}T_f^2 + -5.481717\times10^{-2}RH^2 + 1.22874\times10^{-3}T_f^2RH + 8.5282\times10^{-4}T_fRH^2 + -1.99\times10^{-6}T_f^2RH^2 \quad (2.25)$$

T_f is the temperature in Fahrenheit, and *HI* is also in Fahrenheit. There are a series of assumptions that are made in this calculation. The equation assumes a walking person in shorts and T-shirt, who is male and ~147lbs (Rothfusz, 1990). Additionally, this subject is not in direct sunlight. As with *AT*, *HI* represents a 'feels like' temperature, based upon a level of discomfort.

HUMIDEX was developed by the Meteorological Service of Canada to describe the 'feels like' temperature for humans (Masterson and Richardson, 1979). The original equation used dew point, rather than humidity. The equation has been modified to use vapour pressure, instead:

$$HUMIDEX = T_c + \frac{5.}{9.} * \left(\frac{e_{RH}}{100.} - 10.\right) \quad (2.26)$$

where the *HUMIDEX* is unitless, because it is recognized that the index is a measure of heat load. The warning system has a series of thresholds: 30 is discomfort, 45 is dangerous, and 54 is heat stroke imminent.

The Temperature Humidity Index for Comfort (*THIC*) is a modification of the Temperature Humidity Index (Ingram, 1965). Comfort was rationalized for both humans and livestock through *THIC* (NWSCR, 1976). The index is unitless and is as follows:

$$THIC = 0.72T_w + 0.72T_c + 40.6 \quad (2.27)$$

where the wet bulb temperature (T_w) and dry bulb temperature (T_c) are both in Celsius. The index is used to describe behavioral changes in large animals due to discomfort (seeking shade, submerging in mud, etc.). Additionally, there different approaches to the development of the *THIC*, including considerations of physiology.

2.7.2 Physiology Algorithm

Numerous metrics are based upon direct physiological responses within humans and animals, however almost all of them are complex algorithms (e.g. Moran et al., 2001; Berglund and Yokota, 2005; Gribox et al., 2008; Maloney and Forbes, 2010; Havenith et al., 2011; Gonzalez et al., 2012; Chan et al., 2013). The metrics require radiation measurements, as well heart rate, and even a sweat rate. Therefore, the available metrics that are calibrated for physiological responses and that use meteorological only inputs are limited.

The Temperature Humidity Index for physiology (*THIP*) is one such metric:

$$THIP = 0.63T_w + 1.17T_c + 32. \tag{2.28}$$

where the temperature inputs are the same as in equation 2.27 (Ingram, 1965). *THIP* and *THIC* are generalized equations in the form of:

$$THI = aT_w + bT_c + c \tag{2.29}$$

where the constants *a*, *b*, and *c* (not to be confused with variables in equations from section 2.6) are adjusted for the particular livestock animal. These constants are also based upon physiology or comfort (Lucas et al., 2000). *THIP* is based upon the core temperatures of large animals. Both *THIP* and *THIC* use the same scale for determining qualitative threat levels: 75 is Alert, 79-83 is Dangerous, and 84+ is Very Dangerous. Heat stress *THIP* and *THIC* threshold levels are computed from both outdoor and indoor atmospheric variables. The differences between outdoor and indoor values are used to evaluate evaporative cooling mechanisms, e.g. swamp coolers (Gates et al., 1991a,b).

2.7.3 Empirical Algorithms

Empirically based algorithms measure heat stress through first principle physics, or monitor changes to work loads. Many empirically based algorithms are used for measuring heat stress, such as swamp cooler efficiency. Like the physiology based indices, many empirical algorithms involve metrics beyond atmospheric variables. Many of these empirical algorithms have been simplified for the express purpose of using just atmospheric variables. These simplified versions are widely used, however, In many cases, the calculations are impossible to derive indirectly. For example, natural wet bulb

temperature (Brake, 2001)—dependent on radiation transfer, wind speed, and evaporation—can have up to three different values in convective environments (Alfano et al., 2012). We choose atmospheric variable empirically based heat stress metrics that do not have multiple end members. These metrics either use the Davies-Jones (2008) T_w, or have eliminated the end member issue through their empirical algorithm.

One commonly used empirically derived metric that has not been widely tested is the Simplified Wet Bulb Globe Temperature (*sWBGT*). *sWBGT* is based upon the Wet Bulb Globe Temperature (*WBGT*) that was developed as a decision making tool for the United States Marine Corps (Minard et al., 1957). The *WBGT* uses a combination of wet bulb and dry bulb temperatures as well as a globe thermometer.

$$WBGT = 0.7T_w + 0.2T_g + 0.1T_c \tag{2.30}$$

A globe thermometer (T_g) is a black painted copper globe with a thermometer placed at the center, and measures a combination of radiation and advection temperatures. Due to the complicated nature of calculating/measuring wet bulb temperatures and globe thermometers (it can take 30 minutes for a globe thermometer to reach equilibrium), the *sWBGT* does away with both wet bulb and globe thermometer, entirely. *sWBGT* was designed for estimating heat stress in sports medicine, has been adopted by the Australian Bureau of Meteorology, and is acknowledged that its accuracy may be questionable (ABOM, 2010; ACSM, 1984; ACSM, 1987).

$$sWBGT = 0.567T_c + \frac{0.393e_{RH}}{100.} + 3.94 \tag{2.31}$$

where *sWBGT* is unitless. Thus despite its name, *sWBGT* does not in any way make use of wet bulb temperature.

Discomfort Index (*DI*) has had a similar development history as the *WBGT*. The index was developed in the late 1950s (Thom, 1959), and is used by the Israeli Defense Force as a decision making tool regarding heat stress (Epstein and Moran, 2006). *DI* requires wet and dry bulb temperatures. The computation of wet bulb temperatures in the past has been difficult, and the *DI* equations often have used approximations:

$$T_{wS} = T_c * atan(0.151977\sqrt{RH + 8.313659}) + atan(T_c + RH) - atan(RH - 1.676331) + 0.00391838RH^{3/2} * atan(0.023101RH) - 4.686035 \quad (2.32)$$

where T_{wS} is the wet bulb temperature in Celsius (Stull, 2011). Stull's function has limited range of effective accuracy.

$$\begin{gathered} -20 < T_c < 50 \\ T_c(-2.27) + 27.7 < RH < 99 \end{gathered} \quad (2.33)$$

where not only is the function dependent on temperature, but also minimum *RH* is also function of temperature. *DI* is calculated from these inputs:

$$DI = 0.5T_w + 0.5T_c \quad (2.34)$$

where the *DI* is unitless.

The last index we present is a measurement of the capacity of evaporative cooling mechanisms. Often, these are referred to as swamp coolers. Large scale swamp coolers generally work by spraying a 'mist' into the air. This mist then comes in contact with the skin, and is then evaporated, thus cooling down the subject. In very dry environments, they can be an effective mass cooling mechanism. Unfortunately, they

also raise the local humidity considerably, reducing the effectiveness of direct evaporation from the skin. Swamp coolers are measured by their efficiency:

$$\eta = \frac{T_c - T_t}{T_c - T_w} * 100\% \tag{2.35}$$

where η (%) and T_t is the target temperature for the room to be cooled towards in Celsius (Koca et al., 1991). The maximum efficiency of typical swamp coolers is 80%, and a typical value of a sub-standard mechanism is 65%. Rearranging 2.35 and solving for T_t:

$$T_t = T_c - \frac{\eta}{100}(T_c - T_w) \tag{2.36}$$

where now T_t is the predicted temperature based upon environmental variables. With the mist injected air cooled to T_t, T_t is approximately equal to a new local T_w. Humid environments, or environments that are hot and have an above average *RH*, severely limit the cooling potential of swamp coolers. The following table summarizes the calculated variables and metrics.

Table 1

Moist Temperature Variables and Heat Stress Metrics				
Variable or Metric Name:	**Variable or Metric:**	**Equation #:**	**Output:**	**Calculated:**
Wet Bulb Temperature	T_w	*2.22*	*X*	*X*
Wet Bulb Temperature, Stull	T_{wS}	*2.32 2.33*	*X*	*X*
Lifting Condensation Temp.	T_L	*2.2*		*X*
Moist Potential Temp.	Θ_{DL}	*2.3*		*X*
Equivalent Pot. Temp.	Θ_E	*2.4*	*X*	*X*
Equivalent Temperature	T_E	*2.5*	*X*	*X*
Heat Index	*HI*	*2.25*	*X*	*X*
Apparent Temperature	*AT*	*2.24*	*X*	*X*
Wet Bulb Globe Temp.	*WBGT*	*2.30*		
indoor WBGT	*indoorWBGT*	*2.37*		
Universal Thermal Climate Ind.	*UTCI*	*N/A*		
Simplified WBGT	*sWBGT*	*2.30*	*X*	*X*
Discomfort Index	*DI*	*2.34*	*X*	*X*
Temp. Humidity Index for Comfort	*THIC*	*2.27*	*X*	*X*
Temp. Hum. Index for Physiology	*THIP*	*2.28*	*X*	*X*
Swamp Efficiency 65%	*SWMP65*	*2.36*	*X*	*X*
Swamp Efficiency 80%	*SWMP80*	*2.36*	*X*	*X*
saturated vapor pressure	e_s	*2.13*		*X*
derivative sat. vap. Pressure	de_s/dT	*2.16*		*X*
log derivative sat. vap. press.	$d(ln(e_s))/dT$	*2.15*		*X*
mixing ratio	r_s	*2.14*		*X*
derivative mixing ratio	dr_s/dT	*2.17*		*X*
function of Equiv. Pot. Temp.	$f(\Theta_E)$	*2.18*		*X*
derivative of Equiv. Pot. Temp.	$f'(\Theta_E)$	*2.20*		*X*

2.8 Human Experiences With Heat Stress

Frequent heat waves and prolonged heat stress are concerns for future climate scenarios (Jendritzky and Tinz, 2009; Sherwood and Huber, 2012; SREX IPCC, 2012). Heat stress metrics (i.e. the metrics that involve both heat and humidity) have largely been studied on a sub regional scale. From a climate perspective, these studies have focused on heat waves. The definition of a heat wave, however, has not been consistently defined. The United States National Weather Service initiates heat wave

warnings when *HI* is expected to rise above 40.5°C for two consecutive days (NWS, 2012). Another definition is the characterization of air masses to determine extreme heat (Kalkstein and Greene, 1997). The air masses that denote potential heat threats are 'moist tropical hot', 'dry tropical hot', and are a qualitative estimate of heat waves. The deadliest heat wave on record was the 2010 heat wave in Russia (Dole et al., 2011). The 2003 European and 1995 Chicago heat waves show that heat deaths are related to prolonged exposure to heat stress, not instantaneous exposure (Beniston, 2003; Semenza et al., 1996; Whitman et al., 1997). However, deaths are not the only threat from heat stress. Human work load and worker production rates are intrinsically linked to environmental conditions. The following is a characterization of recent research.

2.8.1 Mortality and Morbidity

Much of the research on heat stress assesses the impacts of heat waves on humans through mortality and morbidity. The focus of these studies is on small regions or cities. For the Chicago heat wave in 1995, research has focused on calculating the odds of mortality based upon a variety of factors. Your odds of death were 8:1 if you were confined to bed, whereas living in an environment with an air conditioner reduced the odds to 0.3:1 (Semenza et al., 1996). Another study teased apart demographics in cities, such as racial background, education, whether the person died in a hospital or not, among other factors., and concluded that for the United States, mortality from heat falls disproportionately to the socially disadvantaged (O'Neill et al., 2003).

Rather than look at mortality, a recent study focused on morbidity and the impact on hospital admissions from heat stress (Li et al., 2012). The authors found that there is a significant relationship to temperature and hospital admissions. The study also found that a variety of conditions are not necessarily correlated to heat stress (e.g. accidents and injuries). The authors took the results further, and used late 21st Century climate model predictions to model the change of hospital admissions to determine how hospitals may be impacted in the future. They concluded people that have preexisting conditions have substantially higher risk to heat in the future.

Heat related medical conditions from working with chronic heat exposure is an exploratory field. Chronic kidney disease rates have substantially increased in Nicaragua (O'Donnell et al., 2011), and there has been no isolated cause of the condition. However, numerous studies show the linking factor between the majority of chronic kidney disease cases are due to frequent exposure to high heat environments (Crowe et al., 2009; Cortez, 2009; Crowe et al., 2010). The focus regionally is to characterize these high heat work environments (Sheffield, 2013). Future predictions are estimating a 15% increase in exposure to high heat stress days in the region.

2.8.2 Heat Stress, Labor Productivity, and Climate Change

The first global assessment of heat stress and its impact on human labor was recently published (Kjellstrom et al., 2009). The study used daily averages GCM output of *RH* and T_c to calculate *sWBGT*. Although the study does not capture the diurnal cycle (therefore, losing the extremes), and neglects the impacts of radiation (by not using

WBGT). The authors were interested in long term averaged future heat stress. The GCM output were the years 1961-1990 (the baseline), 2010-2039, 2040-2069, and 2070-2099 for both a low and high CO_2 concentration increases. Worker productive capacity is a function of metabolic work rate and *sWBGT*. The study uses *sWBGT* to calculate world productivity loss due to climate change at each time slice and CO_2 concentration. The results show that some regions lose up to 25% of their productive capacity (e.g. South East Asia), and other regions lose up to 20% of their Gross Domestic Product (e.g. Central America). Kjellstrom et al. (2009) laid down the groundwork for future global studies on heat stress.

Total and effective labor capacity were calculated in a recent study (Dunne et al., 2013). The study used the monthly output from the Geophysical Fluid Dynamics Laboratory (GFDL) Earth System Model (ESM2M) (Dunne et al., 2013), failing to capture diurnal and daily extremes. Two major results come from this study. 1) In the high CO_2 simulation, by the year 2200, peak labor capacity during the warm season is less than 50% of the total potential labor capacity. 2) Prior to 2010, the authors calculated that there has been a drop in potential labor capacity, to 90%, due to climate change. The authors use *WBGT* as their choice of metric, but with some caveats. The calculation of T_w uses the latest advanced computation (Davies-Jones, 2008) that was used in Sherwood and Huber, 2010. The authors then assume that the workers are in the shade (which is not an unreasonable assumption), however, the authors then assume that the globe temperature is equivalent to the dry bulb temperature:

$$indoorWBGT = 0.7T_w + 0.3T_c \quad (2.37)$$

The resulting equation may have the most accurate calculation for T_w, however, the overall *WBGT* equation is one of the most criticized forms, *indoorWBGT* (Budd, 2006) from lack of radiation and no calibration.

2.8.3 Regional and Global Climate Heat Stress

Climate modeling has recently recognized the importance of characterizing heat stress (e.g. accounting for both moisture and temperature). The focus, however, was still on regional studies. One of the first major modeling studies focused on the Mediterranean (Diffenbaugh et al., 2007). The study uses offline output from a regional model to calculate *HI*. Summer seasonal average *RH*, and daily minimum and maximum temperatures were used to calculate *HI*. Although the *HI* extreme values are less accurate (i.e. the inputs do not capture the daily diurnal cycle), the high CO_2 cases show that there is 3x the number 95th percentile (relative to today) events of high heat stress for the Mediterranean region.

The next global study aimed to set a theoretical framework from which all future research on heat stress must consider. This study used a first principles framework to calculate a physical limit to human adaptive capabilities in heat stress (Sherwood and Huber, 2010). The authors calculated a upper boundary physical energy balance limit that a human at rest will perish–35°C T_w–and then proceeded to calculate a plausible worst case climate change scenario. Their results show that if CO_2 concentration into the atmosphere continues to grow for the next century, 50% of the world where people

live today will become inhabitable at some point on an average year. The only way to maintain homeostasis in these regional zones would require air conditioning.

Incorporating simplified heat stress metrics into an Earth system model was first accomplished with the Community Climate System Model (CCSM4) developed at NCAR (Fischer et al., 2012). This paper moved the field forward in that not only did they couple a heat stress metric to CCSM4 (*sWBGT*), but set out to determine climate change's impact on urban environment, an environment critical to humans. Their results show that extreme heat stress metrics are more spatially uniform than correlating to extreme temperatures. The major conclusion was that the nightly minimum in the urban heat stress rises faster than the daily high within the context of climate change. Specifically, more than half of the nights in Africa and tropical Asia had extreme heat stress when compared to the year 2000 hottest 4 days baseline.

Heat stress metrics, due to the conservation of energy and entropy, inherently reduce the uncertainties of Earth system modeling (Fischer and Knutti, 2012). The study used 4x daily output from both reanalysis and the Climate Model Inter-comparison Project 5 (CMIP5, the latest state of the art climate models), and calculated T_E and *sWBGT*. Results show that the climate models and reanalysis fall along lines of constant T_E even out to the 99th percentile. The result is important because even though scientists have been adding complexity to climate models for decades, the uncertainty of climate predictions remains high. Using a heat stress metric, rather than temperature, has the potential to reduce inter model spread in future predictions.

Finally, have a study was conducted contrasting heat stress changes between rural areas and differing urban densities (Oleson et al., 2013). This study uses *sWBGT*, *DI*, *AT*, *HUMIDEX*, and *HI* (e.g. sections 2.7.1 and 2.7.3), and runs a modern day control simulation compared to a mid-21st century future scenario. Additionally, the study uses numerical downscaling (weather forecasting models) for higher resolution. The boundary conditions were from the Community Climate System Model 4 (Oleson, 2012) and were fed to the Weather Research Forecasting model (Shamarock and Klemp, 2008). The focus was on a variety of cities, given the simulations are limited by both computing power and using a single model. The results show that the urban heat island effect is still larger than the rural area when accounting for moisture. Additionally, the subsequent increases in urban density only have a minor increase in heat stress relative to lower density urban areas.

Although a lot of progress has been made in the short time period that heat stress metrics have appeared in the Earth system model framework, there are some substantial hurdles to overcome. None of the heat stress metrics used in these global studies accounts for radiation impacts on humans, thus limiting the predictive capability. Furthermore, human physiology is a complex system with non-linear responses. Additionally, of all the previously mentioned studies, only two, Fischer et al. (2012), and Oleson et al. (2013), use metrics that were coupled to a simulation, however, very few metrics are calculated. The following section is our method of research to tackle coupling human physiology with Earth systems models.

3. METHODOLOGY

The initial stages of designing algorithms for heat stress built upon previously completed research. Thermodynamic water calculations, and their accuracy are imperative to accurately assessing impacts of heat on humans. The design of analysis tools to assess, describe, and interpret heat stress, additionally, require careful consideration. The focus of this research is on extreme events within the global modeling framework. The tools that have been developed are designed to isolate the top 5% and 1% of events on a yearly basis (~18 days and ~4 days, respectively, per year), and cross compare them between their inputs to the calculation, as well as with each other heat stress metric. We designate the series of FORTRAN90 modules described in this thesis the Human Index Module. The NCAR CESM is coded with FORTRAN language which provides numerous benefits to scientific computing. We present the process of designing the Human Index Module and the tools to analyze the output.

3.1 Design of the Human Index Module

There are three philosophical aspects to the design of the Human Index module presented. 1) The improvement of thermodynamic quantities regarding water, 2) reproduction of previous work, and 3) modular format to increase use through both

narrowly focused applications up to broad based studies. The module itself is in open an source format, and is incorporated into the CLM4.5 developer branch (personal communication, Keith Oleson). The modular format also encourages adapting the code base to specific needs: whether that focus is on improving calculations of thermodynamic quantities or heat stress. The inclusion of heat stress metrics covering comfort, physiology, and empirical design philosophies encourages its use for wide series of applications. The following sections are on the design and implementation of the Human Index Module.

3.1.1 Initial Code Base

Thermodynamic water quantities and their calculation is a crucial step to attempting to understand human heat stress. We use the same limited scope calculation of the Davies-Jones (2008) wet bulb calculations used in Sherwood and Huber (2010). The rationale was that our study of human heat stress realistically only needed to look at the warmest of thermodynamic conditions, and not the entire atmosphere. We could quickly adapt the code base for human applications.

We adapted the original Interactive Data Language (IDL) code (from Steve Sherwood), and translated it into both the NCAR Command Language (NCL) and FORTRAN90 (the code base structure in CLM). The IDL codebase was only valid for wet bulb and equivalent temperatures, as well as, equivalent potential temperature (equation 38 c.f. Bolton, 1980) above the freezing point of water. Additionally, the core vapor pressure calculations are based upon the parameterizations used widely

throughout many general circulation models (Flatau et al., 1992). We applied the code to a testing framework, verifying that the results were duplicated between all three codebases (IDL, NCL, and FORTRAN90).

3.1.2 CLM Implementation

The code was directly implemented into the CLM architecture. Four CLM modules are required to be modified to implement the Human Index module into the land model. These modules were the Bare Ground, Canopy, and Lake fluxes, as well as the Urban Canyon model. We wanted the heat stress calculation to be in any environment that humans could be in. Due to the design of sub-grid scale architecture, implementation must occur simultaneously. The reason for this is that a single grid cell within CLM is made up of up to all four module types. At the end of a time step calculation, the area weight of the different sub-grid cell calculations is averaged together, and then sent off for archival. The design of CLM is such that urban and rural components may be also archived separately for intercomparison. The calculations themselves use the CLM 2 meter calculations of water vapor, temperature, and pressure.

There were some structural issues in the implementation of the wet bulb, equivalent, and equivalent potential temperature calculations into CLM. This is due to memory allocation, and call routines within whole CESM Fortran framework. These were the clmtype (declaration of variable memory), clmtype initialization (initial values, if any), and the history fields (storage) modules. To resolve these issues we used code framework that NCAR used to implement other heat stress routines (personal

communication from Keith Oleson) (Fischer et al., 2012; Oleson, 2013). The code we received demonstrated how to set up the memory allocation (clmtype), initialize values ('not a number'–NaN), and how to pass the variables to storage within netcdf file formats.

The modules provided by Keith Oleson added 5 additional heat stress metrics (*sWBGT*, *DI*, *AT*, *HUMIDEX*, and *HI*). A new design approach was necessary for continued development of the implementation of heat stress within the climate model framework. Any modification necessary to the heat stress code needed to be propagated into all modules. The easiest way to conquer this issue was to pull all of the heat stress routines out of the Bare ground, Canopy, and Lake fluxes, as well as, the Urban modules. A entirely new module and subroutine was developed following the guidelines for module development in CESM.

The heat stress module was split into two subroutines. The first routine calculated the limited scope (above freezing) thermodynamic water related quantities. The second routine calculated the 5 heat stress metrics that NCAR had provided. In the Bare ground, Canopy, and Lake fluxes, and the Urban modules, call routines were introduced that called the two subroutines in the heat stress module. This framework ensured that any modification to the heat stress module would be propagated to all subsequent CLM rountines. Additionally, multiple forms of *DI* are computed. NCAR implemented T_{wS} (Stull, 2011), and calculating the differences between our T_w thermodynamic routine and NCAR's T_{wS} routine was added.

The module routines were thoroughly tested within the CESM framework using the Community Atmospheric Model (Gent et al., 2011; Song et al., 2012) and with the use of reanalysis data product ERA Interim (Dee et al., 2011). At the time for submission for official implementation into the CESM, NCAR required that all code that is to be added to the codebase must be robust for a wide range of applications. With the afore mentioned calculations only valid over above freezing conditions, the module was severely limited scope. Reevaluation of the thermodynamic routines was required.

We implemented the entirety of the thermodynamic routines developed by Davies-Jones (2008) into a new module called the HumanIndexMod. Additionally, this required using an entirely different calculations for Θ_E (equation 2.4). Equation (2.4) is the most accurate and efficient Θ_E calculation available (Bolton, 1980; Davies-Jones, 2009). To calculate equation. (2.4) required implementing T_L and Θ_{DL}, equations. (2.2) and (2.3), respectively, into the HumanIndexMod. The accelerated Newton-Raphson method used in our original routine was only valid for the IDL codebase equations. We implemented the full Newton-Raphson equation (2.22), which is dependent on eqs. (2.9-2.21).

The thermodynamic water vapour calculations within CESM are calculated within a separate routine called QSat. These calculations use polynomial fits to the Clausius-Clayperon vapour calculations (Flatau et al., 1992). They were designed to be computationally fast at the expense of being extremely accurate during a time when computing power was limited. 20 years have gone by since these calculations were last updated. Equations (2.13-2.17) use the August-Roche-Magnus equation, considered to

be one of the most accurate calculations for saturation vapour pressure. Calculating the August-Roche-Magnus equation and subsequent related equations for T_w, we created a subroutine, QSat_2, that calculated all the same functionalities as QSat, but using the August-Roche-Magnus equation. Additionally, we have added the $f(\Theta_E)$ with respect to the input temperature, and the subsequent derivatives. This opens up opportunities for researchers to replace QSat with QSat_2 (i.e. replace saturated vapour calculations with the accurate calculations). Additionally, QSat_2 is robust over a larger range of conditions in the atmosphere as compared to QSat.

We found it is advantageous to split every single heat stress quantity into its own subroutine. Two forms of *THI* (*THIC* and *THIP*), as well as Swamp Cooler Efficiency (*SWMP65* and *SWMP80*), were added to the list of metrics in the Human Index module. Many heat stress quantities required T_c and others needed e_{RH}; we added two routines that will calculate those quantities.

The Human Index module was designed such that the minimum requirements to calculate all of the metrics were *T* (K), *P* (Pa), *RH* (%), specific humidity (g/kg), *e* (Pa), and u_{10m} (m/s). We left the user with the choice of what quantities to be calculated, increasing the flexibility of computation for those with narrow or broad based needs. Table 2 shows the complete list of quantities that are calculated in the Human Index module, and which subroutine calculate these quantities.

Table 2

Human Index Module			
Name	**Subroutine:**	**Requires:**	**Calculates:**
Moist Thermodynamics	*Wet_Bulb*	$T\ e_{RH}\ P\ RH\ Q$	$T_E\ \Theta_E\ T_w$
Wet Bulb Temp. Stull	*Wet_BulbS*	$T_c\ RH$	T_{wS}
Heat Index	*HeatIndex*	$T_c\ RH$	*HI*
Apparent Temperature	*AppTemp*	$T_c\ e_{RH}$ *Wind*	*AT*
Simplified WBGT	*swbgt*	$T_c\ e_{RH}$	*sWBGT*
Humidex	*hmdex*	$T_c\ e_{RH}$	*HUMIDEX*
Discomfort Index w/Stull	*dis_coi*	$T_c\ T_w$	*DI*
Discomfort Index w/Stull	*dis_coiS*	$T_c\ T_{wS}$	*DI*
Temp. Hum. Index	*THIndex*	$T_c\ T_w$	*THIC THIP*
Swamp Cooler Eff.	*SwampCoolEff*	$T_c\ T_w$	*SWMP65 SWMP80*
Kelvin to Celsius	*KtoC*	T	T_c
Vapor Pressure	*VaporPres*	$RH\ e_s$	e_{RH}
Sat. Vapor Pressure	*QSat_2*	$T\ P$	$e_s\ de_s/dT\ d(\ln(e_s))/dT\ r_s\ dr_s/dT\ f(\Theta_E)\ f'(\Theta_E)$

3.2 Model Design

Our approach to validating the Human Index Module was three-fold. 1) Testing of the HumanIndexMod using reanalysis products at 6 hourly averages. 2) The use of GCMs to capture all of the extremes, and directly calculating these metrics at the time-step interval (30 min). 3) After verifying the calculations have been working properly between both reanalysis and GCMs, we used a hybrid simulation combining reanalysis and GCMs.

3.2.1 Reanalysis

Reanalysis products are general circulation models (GCM) that use data assimilation to incorporate observational datasets. These reanalysis assimilate radar,

surface observations,weather soundings, satellites, and ocean measurements. The data is interpolated to a gridded format and is fed into GCMs at regular intervals. The GCMs, using their fluid dynamical and energy equations, generate the state of the atmosphere. The end result is to generate products for research and weather forecasting that describe the modern state of the atmosphere, through the guise of the assumptions within the particular GCMs producing the product. Note that although driven by observations, reanalysis products are not true observations. We used three different reanalysis products listed in table 3.

Table 3

Reanalysis Products			
Name	**Short Name**	**Ref:**	**This Paper**
European Reanalysis Interim	ERA Interim	Dee et al., 2011	
NCEP-DOE Reanalysis II	R2	Kanamitsu et al., 2002	
CRUNCEP	CRUNCEP	Mitchell and Jones, 2005; Kalnay et al., 1996	X

The first reanalysis product we used was the European Reanalysis Interim project (ERA Interim) (Dee et al., 2011). The product was developed by the European Centre for Medium-Range Weather Forecasts. ERA Interim runs from 1979-2012, and we used the surface outputs for surface pressure, 2m temperature, 2m dew point temperature at 6 hourly averaged intervals with a spectral resolution ~0.5°x0.5°. We convert the dew point temperature into relative humidity using a software package in the NCAR Command Language (NCL). The reanalysis product has improvements over its predecessor (ERA-40) through moist boundary layer treatments, by using conserved

water quantities. ERA Interim is able to capture the intensity of extreme events, such as storms, but has issues with timing (Dee et al., 2011). We largely used this data product for testing purposes.

The second reanalysis product we used is the National Centers for Environmental Prediction-Department of Energy Reanalysis 2 (NCEP-DOE R2, henceforth, R2) (Kanamitsu et al., 2002). R2 runs from 1979-2010 and we used 6 hourly averaged intervals of the lowest model level outputs with a spectral resolution of ~2°x2°. Variables used were: surface solar radiation, surface precipitation rate, temperature, specific humidity, zonal and meridional winds, and surface pressure. The product has significant improvements in data assimilation over the previous product (R1), such as Southern Hemisphere erroneous data problems replaced, new treatments of snow cover, additional satellites, ocean albedo changes, among other things. There are errors, however, in the product: the zonal ozone latitudinal orientation was reversed, and a counter gradient flux formulation (boundary layer eddies), designed for oceans, was applied everywhere (Kanamitsu et al., 2002). The treatments of near surface temperatures and soil moisture have improved. This data product was used for testing purposes.

The CRUNCEP dataset is the last product that we used. It is a combination of the Climatic Reach Unit (CRU) gridded observations dataset from the University of East Anglia (Mitchell and Jones, 2005), and the NCEP/NCAR reanalysis product (Kalnay et al., 1996). The dataset runs from 1901-2010, and is on a regular grid of ~0.5°x0.5°. The combination of CRU and NCEP was to correct for biases in the reanalysis product, and

also improve the overall resolution (Casado et al., 2013). We used the following variables: surface solar radiation, surface precipitation rate, temperature, specific humidity, zonal and meridional winds, and surface pressure. The CRUNCEP is the default data-atmosphere forcing set for the CLM4.5.

3.2.2 CESM Model Setup

We used two types of CESM simulations for testing and implementing the HumanIndexMod. The first configuration was a thermodynamic 'slab' ocean coupled the CAM4/5 atmosphere and CLM4.0. The second configuration was stand alone simulation CLM4.5 forced by CRUNCEP and R2. As with the ERA Interim, the slab ocean configurations were largely for testing purposes. The R2 simulations were for testing purposes, as well. We switched to the hybrid (CLM4.5 forced by reanalysis) approach for the purposes of having 'clean' comparisons between different forcing products and mapping out variability with CLM4.5. Table 4 lists all of the simulations executed.

Table 4

CESM Simulations						
Name	**CESM Version**	**CAM Version**	**CLM Version**	**Type**	**Testing**	**This Paper**
Interglacial 132ka	*1.0.5*	*4*	*CLM4*	*Slab Ocean*	*X*	
Interglacial 244ka	*1.0.5*	*4*	*CLM4*	*Slab Ocean*	*X*	
Interglacial 337ka	*1.0.5*	*4*	*CLM4*	*Slab Ocean*	*X*	
Interglacial 132ka	*1.0.5*	*5*	*CLM4*	*Slab Ocean*	*X*	
Interglacial 244ka	*1.0.5*	*5*	*CLM4*	*Slab Ocean*	*X*	
Interglacial 337ka	*1.0.5*	*5*	*CLM4*	*Slab Ocean*	*X*	
CRUNCEP	*1.2*	*N/A*	*CLM4.5*	*Forced Land*		*X*
R2	*1.2*	*N/A*	*CLM4.5*	*Forced Land*	*X*	
Modern year 2000	*1.0.5*	*4*	*CLM4*	*Slab Ocean*	*X*	
Modern year 2000	*1.0.5*	*5*	*CLM4*	*Slab Ocean*	*X*	
Modern 1120 ppmv CO_2	*1.0.5*	*4*	*CLM4*	*Slab Ocean*	*X*	
Modern 1120 ppmv CO_2	*1.0.5*	*5*	*CLM4*	*Slab Ocean*	*X*	
Pre-Industrial 1850	*1.0.5*	*4*	*CLM4*	*Slab Ocean*	*X*	
Pre-Industrial 1850	*1.0.5*	*5*	*CLM4*	*Slab Ocean*	*X*	
Miocene	*1.0.5*	*4*	*CLM4*	*Slab Ocean*	*X*	
Eocene	*1.0.5*	*4*	*CLM4*	*Slab Ocean*	*X*	

Our test simulations used a configuration called slab ocean. These simulations are given initial and boundary conditions, such as solar radiation, aerosols, among others. The ocean, rather than using dynamical flow equations, becomes a thin layer 'slab' that is a series of heat flux boundary conditions meant to represent the mixed-layer of the global ocean. The heat flux parameters of the ocean are derived from fully coupled dynamical ocean simulations (Goldner et al., 2013) from modern year 2000 boundary conditions. The slab ocean in our experiments are coupled to CAM4 (Gent et al., 2011) and CAM5 (Song et al., 2012), which, in turn, were coupled to CLM4.0 (Lawrence et al., 2011). 4 types of simulations were executed. Two default control runs: 'out of the box' simulations with year 2000 and pre-industrial 1850 boundary conditions.

These simulations were compared with three types of sensitivity runs. Pre-Industrial boundary conditions with different orbital parameters (obliquity, eccentricity, and precession); Paleoclimatic boundary conditions for the Eocene and Micoene epochs; year 2000 boundary conditions with 1120 ppmv CO_2 concentrations. The various renditions of the HumanIndexMod were implemented directly into the CLM4.0 code for these simulations since they were conducted with an earlier version of CESM. The simulations were initialized, and executed until they reached equilibrium, ~30 model years. Afterward, the simulations were extended for an additional 20 years to develop a climatology. The length of time was to account for different modes of variability within the climate system for each simulation.

The second simulation type was an approach using CLM4.5 driven by reanalysis. CLM4.5 was released in July, 2013, and the model had substantial improvements over the previous versions—including improved urban canyon components, as well as new biogeochemical cycles (Oleson et al., 2013). Additionally, it was decided that comparing CLM output with reanalysis required having both systems within the same architecture. CLM4.5 may be forced by just an atmospheric boundary condition (i.e. any model output may be coupled to CLM4.5). We ran two CLM4.5 simulations. The first was CLM4.5 using the R2 reanalysis product (testing), and the second was forced by CRUNCEP forcing dataset.

We chose to run CLM4.5 with the biogeochemical cycles turned on. These simulations represented having every climatic component of CLM4.5 turned 'on'. We followed the model execution format designed by NCAR. The setup of the default

configuration (CRUNCEP) followed a series of steps. The simulation was initialized at 1850, using the boundary conditions provided from NCAR (Sam Levis, personal communication). The simulation was spun up until 1901, looping the CRUNCEP years 1901-1920. Then the simulation used CRUNCEP 1901-1948. At 1949, a different computer system was used for high performance considerations, and the simulation was executed from 1949-2010. The R2 simulation was initialized using the 1949 boundary conditions of the CRUNCEP simulation. This simulation ran until 1978, looping R2 years 1979-1983, to spin up the land model reflecting differences in R2 and CRUNCEP input. Finally, at 1979, R2 was run through 2010. CRUNCEP 1979-2010 is used for analysis, as this is the default configuration used by NCAR.

3.3 Analysis of Heat Stress Indices

Designing a module to calculate human heat stress metrics also requires designing tools to quantify the extreme events that cause human heat stress. There are many approaches to evaluating heat stress. Monthly and seasonal averages were used for general applications (Diffenbaugh et al., 2007; Dunne et al., 2013), however these averages potentially underestimate the potential severity of heat stress. Recent research has used daily values (Kjellstrom et al., 2009; Hyatt et al., 2010), but ultimately, capturing the diurnal cycle is crucial for quantifying heat stress extremes (Oleson et al., 2013). Heat stress related illnesses are exacerbated by high heat stress nights as well as daytime.

We used 4x daily averages from our simulations and from reanalysis. We outputted both the heat stress metrics and the corresponding pressure, temperatures, and relative humidity fields that were inputs for these metrics. The 4x daily output are compiled into yearly files with 1460 time steps. Each year has its statistics computed (mean, variance, exceedance, etc.). This is a special function in the NCL software package. The NCL exceedance package was designed for single point time series analysis for less than 1000 data values. We modified the original package to handle 1000s of values, and calculate over every grid point. The results are a variety of statistical diagnostics. Originally, we focused on the hottest 6 hour period. However, we found an issue in what is suspected to be a parameterization of the bareground land unit (see section 4.1). We shifted focused to the 95th and 99th percentiles (hottest 73 and 15 six-hour intervals, respectively) because the issue with the bareground module was infrequent, even at the 99th percentile.

Every 6 hour period within a year that exceeded the percentiles of that year were located. These spatial-time cubes were used to calculate joint distributions. For example, the 99th percentile of *HI* isolates the top hottest 15 time steps of *HI* in each grid cell. This is then mapped onto the *T* and *RH* for the same corresponding time steps, isolating the components that calculated the *HI*. The 99th percentile of *HI* was also used to isolate all of the other metrics. The joint distributions were applied to all heat stress metrics and inputs variables, allowing for cross comparison between any metric. The aim is to develop an analysis technique comparing of all heat stress metrics within CLM4.5.

After the joint distributions have been calculated, we, again, take the statistical dispersion of the resulting datasets. The result gives us the distribution of the extreme events themselves, as well as the spread in the joint distributions. We develop two methods of displaying the output for visual analysis. The first are world contour plots. These plots are the 95th and 99th percentiles of the metrics and input variables, and the medians of their joint distributions. We chose the medians rather than the means due to the influence of the bareground land unit issue previously mentioned. The other type of plot we use are box and whisker plots. We selected a variety of city localities around the world to both map out heavily populated areas of the world, but also display latitudinal and regional influence on heat stress (Table 5). Due to the variance that an individual grid cell may have, we averaged the statistical dispersion information of all 8 nearest local grid cells to the city location together. We plot the joint distributions. The x-axis is the 95th or 99th percentiles, and the y-axis are the box plots of the joint. The whiskers are the minimum and 90th percentile (not max due to bareground land unit issue), the box edges are the 75th and 25th percentiles, and line is the median. The following section displays some of the metrics and their characterization within CLM4.5.

Table 5

Regional City Location							
CITY:	**LAT:**	**LON:**	**REGIME:**	**CITY:**	**LAT:**	**LON:**	**REGIME:**
Chicago	*41.52*	*-87.37*	*Mid-Latitude*	***Melbourne***	*-37.48*	*144.58*	*Mid-Latitude*
Paris	*48.51*	*2.21*	*Mid-Latitude*	***Caracas***	*10.29*	*-66.54*	*Equatorial*
Moscow	*55.45*	*37.37*	*Mid-Latitude*	***Bangkok***	*13.43*	*100.28*	*Convective*
Beijing	*39.54*	*116.24*	*Mid-Latitude*	***Monrovia***	*6.18*	*-10.47*	*Equatorial*
Singapore	*1.21*	*103.49*	*Equatorial*	***Washington DC***	*38.53*	*-77.02*	*Mid-Latitude*
New Delhi	*28.37*	*77.13*	*Convective*	***New Orleans***	*29.57*	*-90.04*	*Convective*
Islamabad	*33.43*	*73.03*	*Convective*	***Miami***	*25.47*	*-80.63*	*Convective*
Cairo	*30.02*	*31.14*	*Arid*	***Houston***	*29.45*	*-95.22*	*Convective*
Dodoma	*-7.05*	*38.02*	*Equatorial*	***San Francisco***	*37.46*	*-122.25*	*Mid-Latitude*
Darwin	*-12.27*	*130.50*	*Convective*	***Tel Aviv***	*32.03*	*34.46*	*Arid*
Christchurch	*-43.31*	*172.38*	*Mid-Latitude*	***Port Said***	*31.15*	*32.18*	*Arid*
Mexico City	*19.25*	*-99.07*	*Arid*	***Amman***	*31.57*	*35.56*	*Arid*
Rio de Janeiro	*-22.54*	*-43.12*	*Mid-Latitude*	***Beirut***	*33.53*	*35.29*	*Arid*
Tokyo	*35.41*	*139.41*	*Mid-Latitude*	***Damascus***	*33.30*	*36.18*	*Arid*
La Paz	*-16.29*	*-68.08*	*Arid*	***Aleppo***	*36.12*	*37.09*	*Arid*
Jerusalem	*31.46*	*35.12*	*Arid*	***Riyadh***	*24.42*	*46.43*	*Arid*
Rome	*41.54*	*12.27*	*Mid-Latitude*	***Mecca***	*21.25*	*39.49*	*Arid*
Shanghai	*31.13*	*121.28*	*Convective*	***Khamis Mushait***	*18.18*	*42.44*	*Arid*
Chibi	*29.43*	*113.54*	*Convective*	***Medina***	*24.27*	*39.37*	*Arid*
Dhaka	*23.42*	*90.24*	*Convective*	***Buraydah***	*26.20*	*43.58*	*Arid*
Libreville	*0.20*	*9.22*	*Equatorial*	***Dammam***	*26.23*	*49.58*	*Arid*

4. RESULTS

The results we are presenting here are snap shot of the many metrics being calculated. We show an example of the possible global applications for these metrics. Additionally, we break down the analysis into three sections: desert soils, spatial joint distribution plots, and box joint distributions. This approach shows the characterization of heat stress within CLM4.5 in response to one observation reanalysis product, the CRUNCEP.

4.1 Desert Soil Parameterization

CLM4.5 parameterization of the world deserts is based upon the southwestern United States. This region is on the order of ~100k years old, and has developed a calcrete (hardpan) surface layer that is largely impervious to water percolation. When this is applied to desert regions of the world that are made of porous sand (e.g. Saharan Desert, Arabian Peninsula, etc.), rainfall will pool on the surface and evaporate into the near surface layer. The result is a ~6 hour period of time of a given year where the Θ_E is approximately +20K warmer than the top warmest 3 day period (not shown). This result does not occur at the 99th percentile (hottest ~3 days). For this reason, the rest of the results are presented using 95th percentiles rather than model maximums.

4.2 Spatial Joint Distributions of Heat Stress

We present spatial joint distribution plots at the 95th percentile of thermodynamic quantities *Q*, *RH*, *T*, Θ_E, T_w, and two heat stress metrics, *HI* and *THIC*. Each figure (Figures 1 and 2) shows intercomparisons with the other metrics. The figures and text will use the labeling convention of 'B_g_A', where 'A' is a metric and 'B' is the quantity in the in the figure. These spatial plots are an average of the 95th percentiles of each given year (1979-2010; 32 years). Note, no statistical testing was used and the assessment is qualitative. The plots show the average variability between each thermodynamic quantity and heat stress metric. We categorize the spatial distribution plots into two separate categories.

The first category of spatial distributions (Figure 1) are two heat stress metrics (*THIC* and *HI*) and one moist thermodynamic quantity (T_w). These variables are compared to the constituent components (*T*, *RH*, *Q*) that calculated the *THIC*, *HI* and T_w. The spatial distributions between *THIC* and *HI* are similar (Figure 1a, 1e), while they differ from T_w (Figure 1i). The arid regions of the world show a heat stress spatial pattern that is different from the moist thermodynamic quantity. Conversely, the non-arid regions are similar between T_w, *THIC*, and *HI*. The differences are apparent in the joint distributions of *T* (Figure 1b, 1f, 1j). The spatial patterns of *T* show THIC and HI are similar. T_w differs over southern Africa, the Indian subcontinent, and the arid regions of Australia. Spatial patterns of *RH* reflect the differences in *T* between the heat stress metrics and moist thermodynamics (Figure 1c, 1g, 1k). The before mentioned regions have increased *RH* when considering T_w as compared to *THIC* and *HI*. Exploring further,

the differences between the heat stress metrics and the moist thermodynamics is measured by the amount of moisture (Figure 1d, 1h, 1l). T_w scales with Q and their spatial patterns are similar (Figure 1i, and 1l). The regions where T_w differs from *THIC* and *HI* are explained by higher moisture levels for maximum T_w.

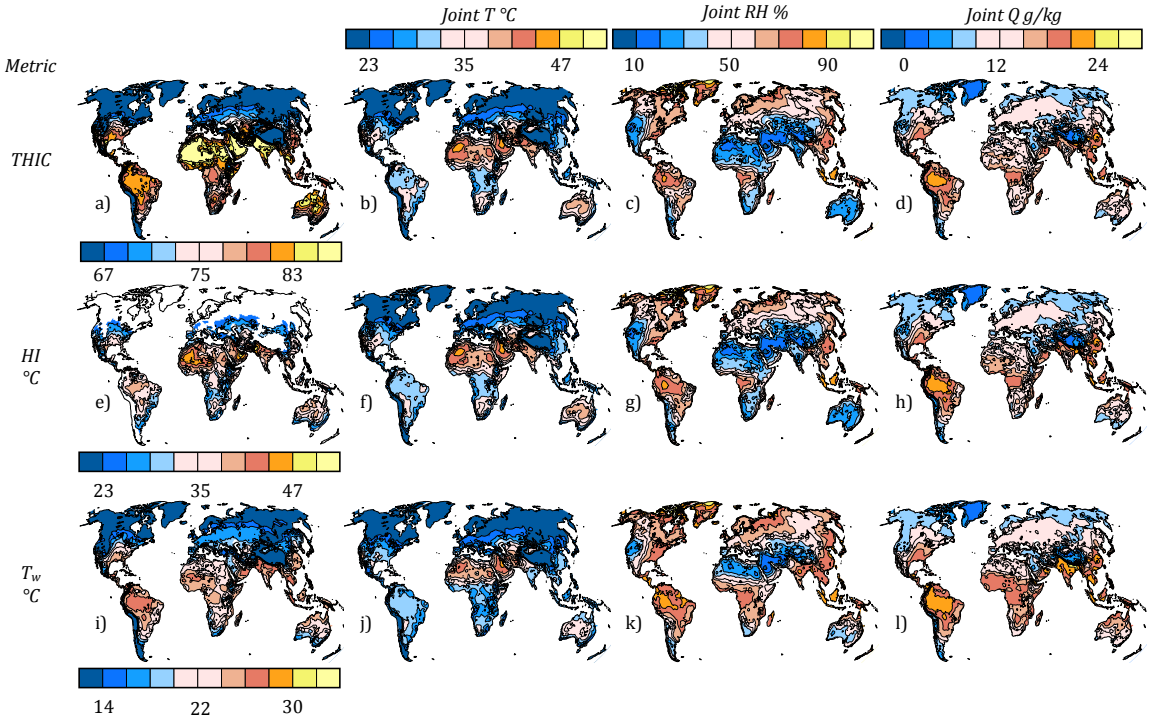

Figure 1: Spatial distributions at the average of the 95th percentile from 1979-2010 CLM4.5 forced by CRUNCEP. a) *THIC*, b) *T_g_THIC*, c) *RH_g_THIC*, d) *Q_g_THIC*, e) *HI*, f) *T_g_HI*, g) *RH_g_HI*, h) *Q_g_HI*, i) T_w, j) *T_g_*T_w, k) *RH_g_*T_w, l) *Q_g_*T_w. a), e), and i) use the color bar underneath their plot, respectively. b), f), and j) use the *Joint T °C* color bar. c), g), and k) use the *Joint RH %* color bar. d), h), and l) use the *Joint Q g/kg* color bar.

The second category of spatial distributions (Figure 2) are an analysis of heat stress metrics and moist thermodynamics as a function of T_w. Additionally, there is an intercomparison of *HI_g_THIC* (Figure 2h). As with Figures 1a, 1e, and 1i, *THIC*, *HI*, and

T_w. are shown for intercomparison (Figure 2b, 2c, and 2g, respectively). Θ_E is a strong function of T_w, and the spatial distribution of T_w dictates the spatial distribution of Θ_E (Figure 1a, 1d). High T_w heavily influences *THIC* and *HI* in specific regions (Figure 2b, 2c, 2e, and 2f). High heat stress in the southern United States and Southeastern China are heavily dependent on T_w. The Indian subcontinent, however, does not have the same level of dependence on T_w in the heat stress metrics. Lastly, we show *HI* as a function of *THIC* (Figure 2h). The spatial patterns between *HI* and *HI_g_THIC* are nearly identical with some minor magnitude differences in the Gulf of Mexico, Amazon Basin, and east of the Caspian Sea.

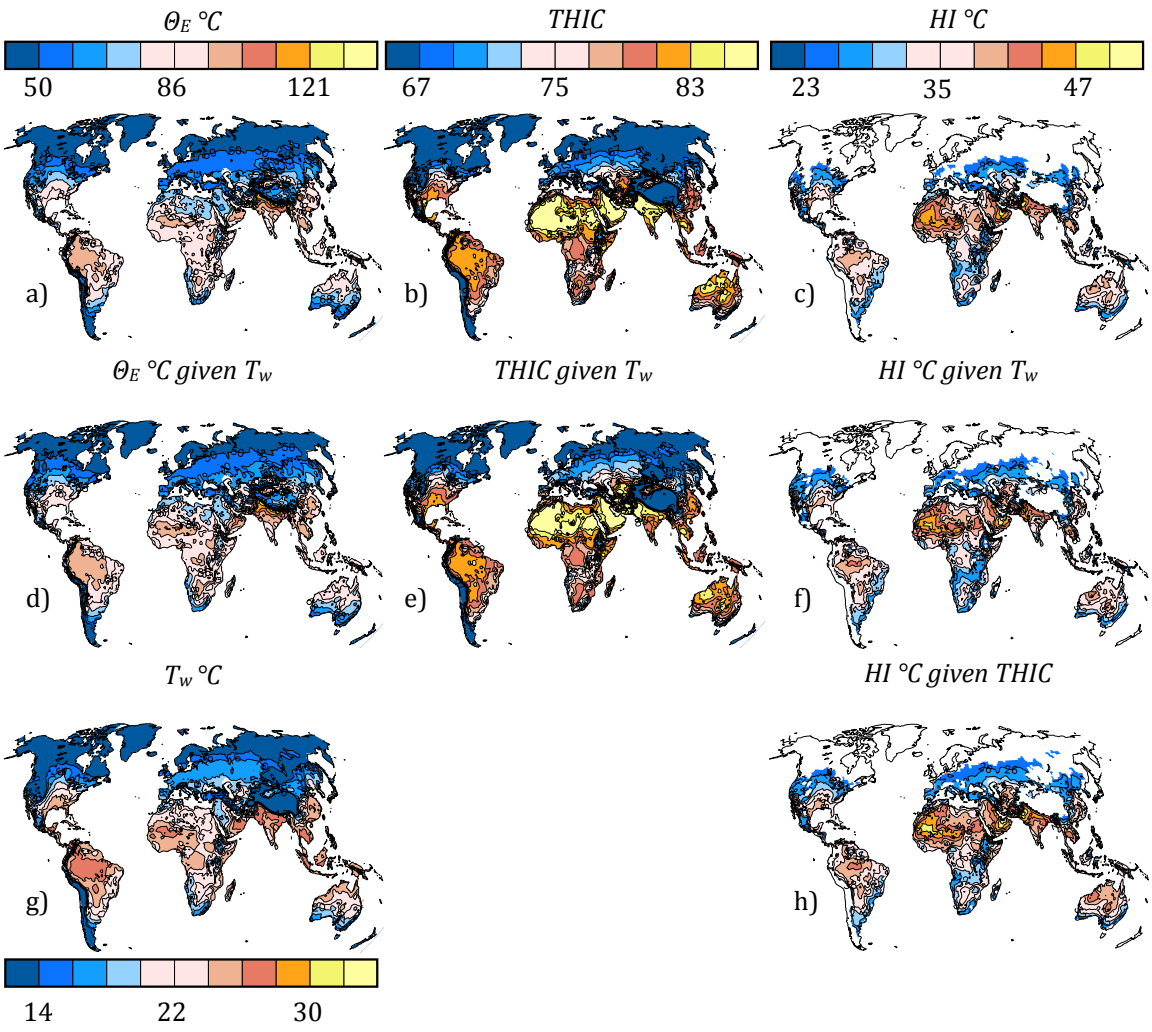

Figure 2: Spatial distributions at the average of the 95th percentile from 1979-2010 CLM4.5 forced by CRUNCEP. a) Θ_E, b) *THIC*, c) *HI*, d) Θ_E*_g_*T_w, e) *THIC_g_*T_w, f) *HI_g_*T_w, g) T_w, h) *HI_g_THIC*. a) and d) use the Θ_E°C color bar. b) and e) use the *THIC* color bar. c), f), and h) use the *HI °C* color bar. g) uses the T_w *°C* color bar.

4.3 Metropolitan Regions and Joint Distributions of Heat Stress

Here we examine regional differences between heat stress metrics and moist thermodynamic quantities. The variability of the magnitude of heat stress is dependent on regional location, which determines whether heat stress is driven by convective processes (latent heat) or non-convective. We use major metropolitan city locations

(Table 5) to simplify the regional analysis and also focus on locations where humans live in large numbers. Additionally, these city locations are grouped by 4 regional similarities: convective (red), equatorial (blue), arid (gold), and mid-latitude (green).

We focus on moist thermodynamic quantities, Θ_E and T_w (Figure 3 and 4, respectively), first. The 95th percentiles of Θ_E and T_w shows the convective regions (±30° latitude) have maximized specific humidity (Figure 3f and 3f, respectively), followed by the equatorial regions. The moisture in mid-latitudes drops off moving away from the equator, and the arid regions have lower specific humidity relative to Θ_E and T_w values. The mid-latitude, equatorial, and convective *T* regions all plot as a latitudinal dependency, while the arid regions are independent of this (Figure 3a and 4a). Likewise, *RH* for mid-latitude, equatorial, and convective regions are consistently ~60-80% with respect to the 95th percentile of Θ_E and T_w (Figure 3b and 4b). The relationship between moist thermodynamic quantities and heat stress metrics breaks down over arid regions (Figure 3c,d and 4d,e). The heat stress metrics are high because the moist thermodynamic quantities are high, however, the heat stress metrics are amplified by high *T*.

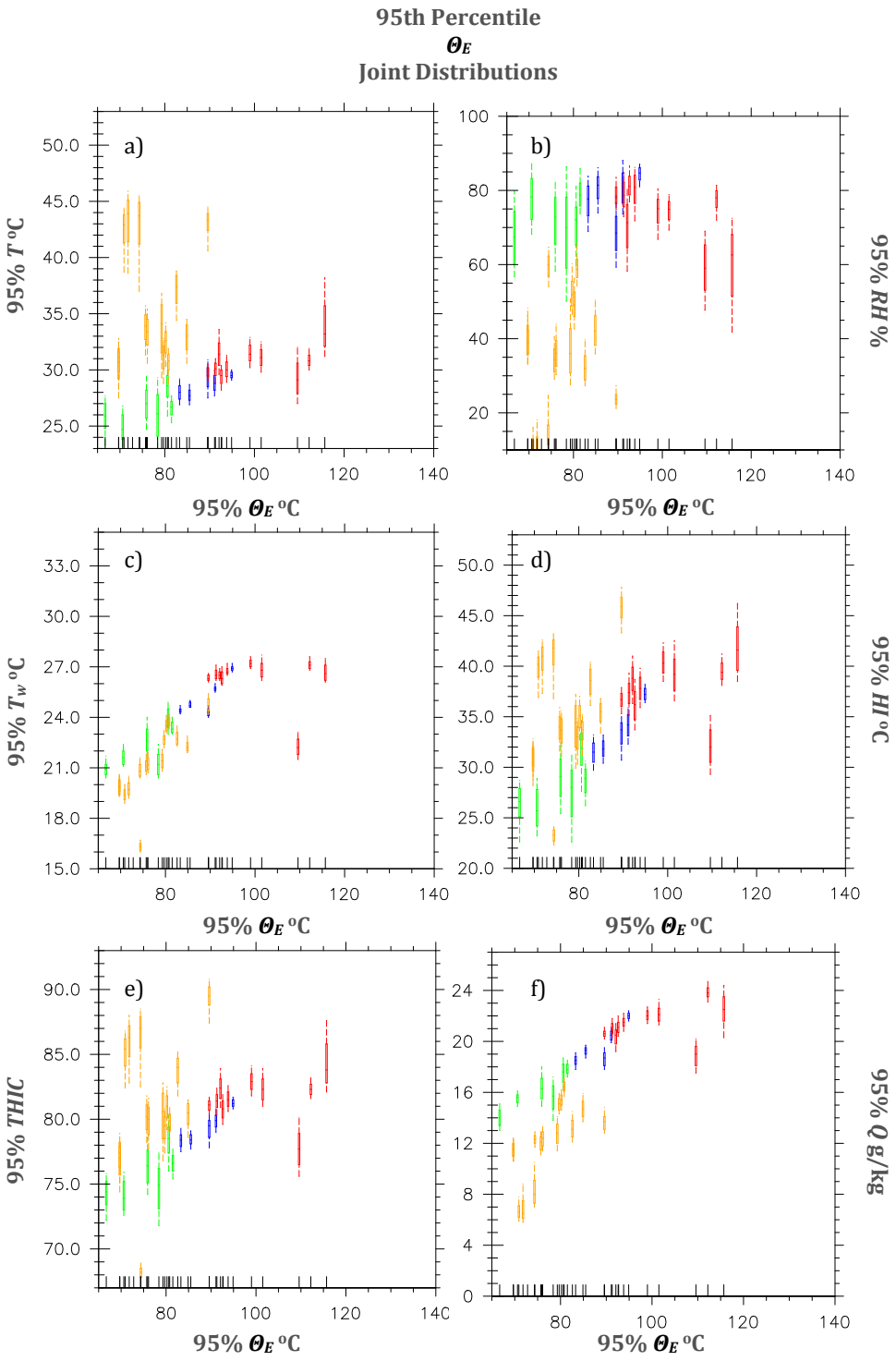

Figure 3: 95th percentile joint distribution box and whisker plots of Θ_E. Each box and whisker plot is a metropolitan area location. The colors represent different regional associations: convective (red), equatorial (blue), arid (gold), and mid-latitude (green). The joints with respect to equivalent potential temperature are: a) *T*, b) *RH*, c) T_w, d) *HI*, e) *THIC*, and f) *Q*.

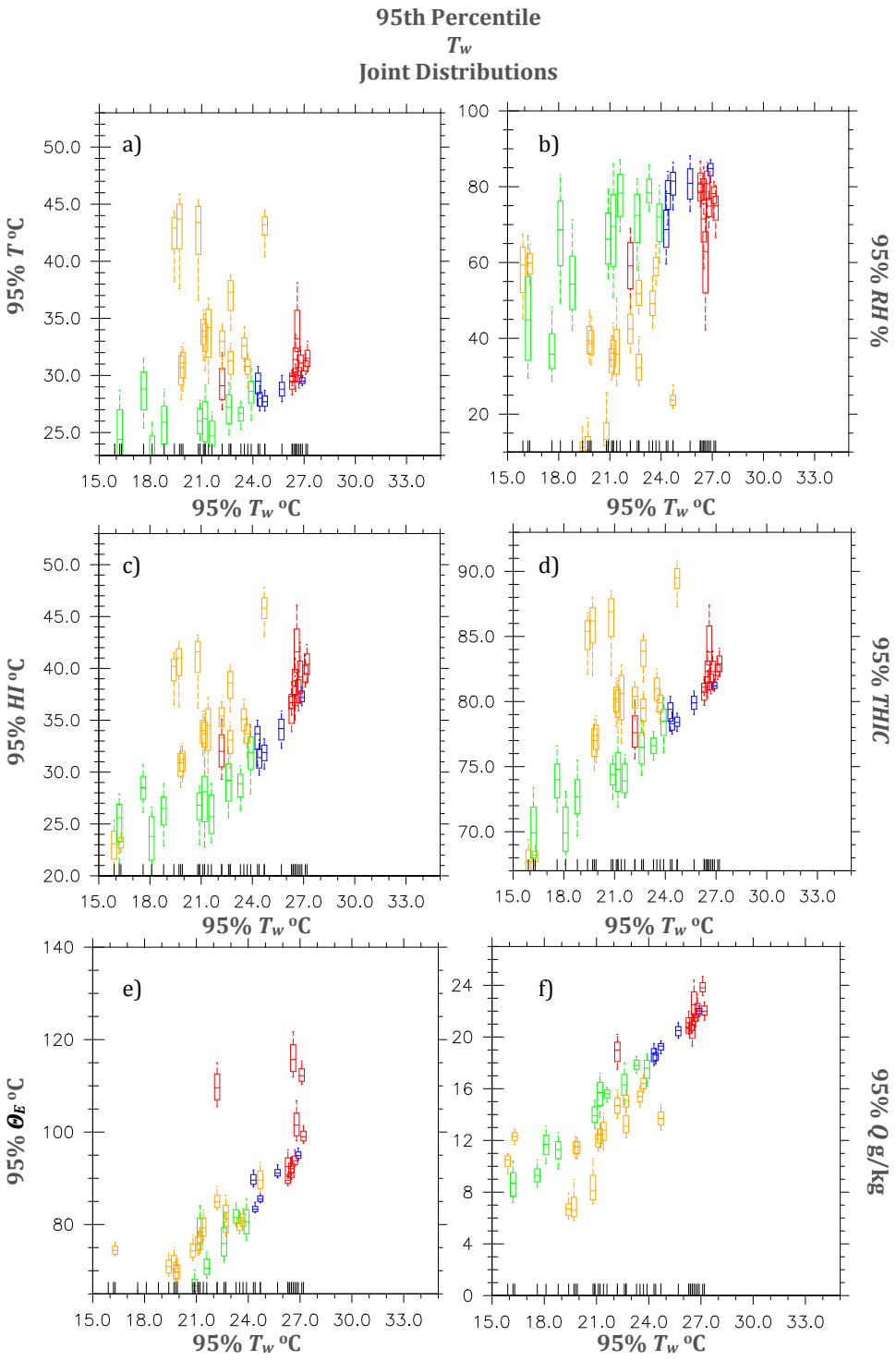

Figure 4: 95th percentile joint distribution box and whisker plots of T_w. Each box and whisker plot is a metropolitan area location. The colors represent different regional associations: convective (red), equatorial (blue), arid (gold), and mid-latitude (green). The joints with respect to wet bulb temperature are: a) *T*, b) *RH*, c) *HI*, d) *THIC*, e) Θ_E, and f) *Q*.

Heat stress metrics show different characteristics than the moist thermodynamic quantities. Convective regions show that small variations in T_w can lead to large variations in the heat stress (Figure 5c and 6c). Additionally, the arid region *T* drive the 95th percentile of heat stress metrics (Figure 5a and 6a). *RH* in the arid regions has small variability as compared to other regions at high heat stress (Figure 5b and 6b). Additionally, there is a near linear correlation between heat stress metrics *HI* and *THIC* (Figure 5d and 6d).

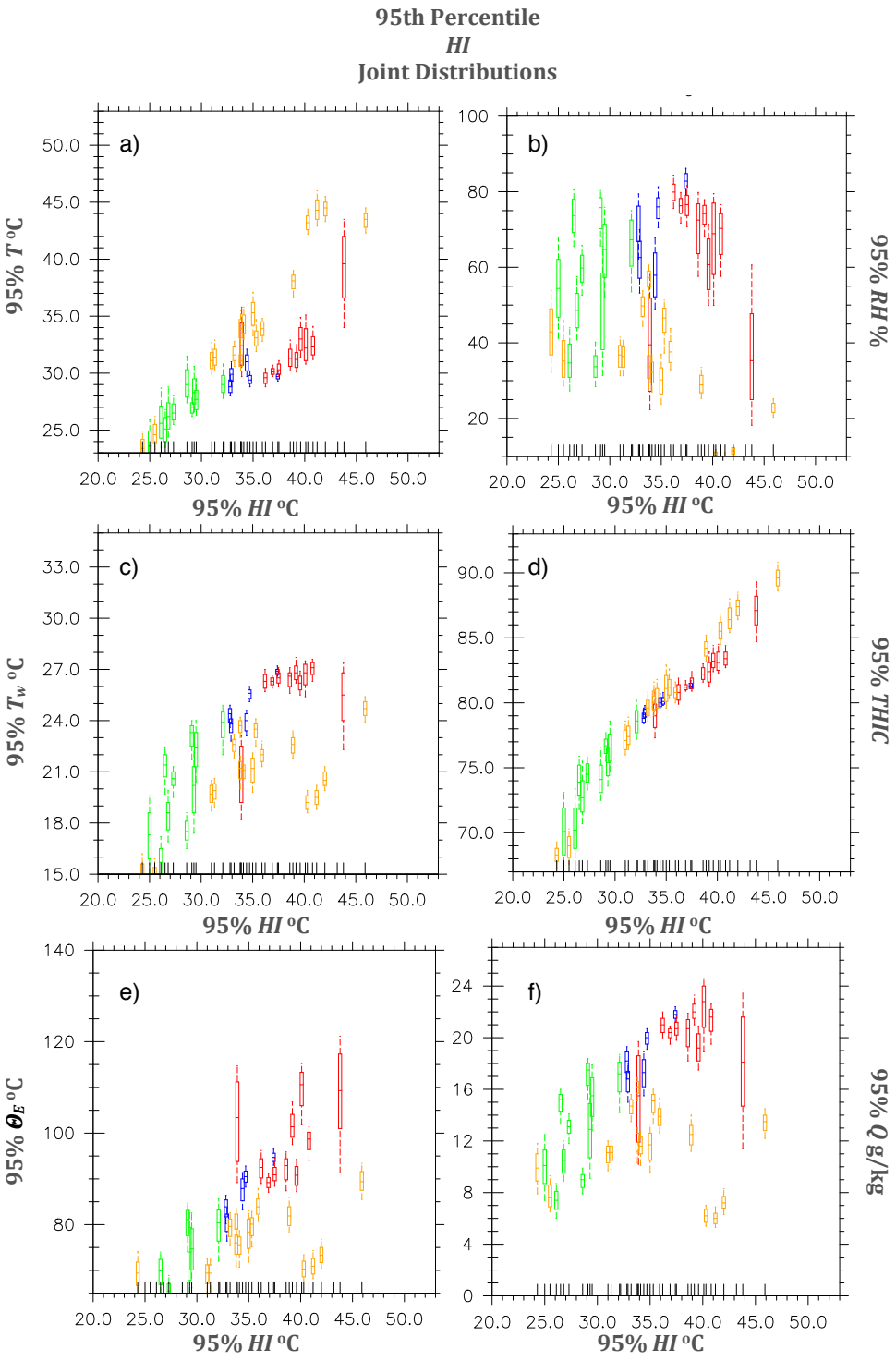

Figure 5: 95th percentile joint distribution box and whisker plots of *HI*. Each box and whisker plot is a metropolitan area location. The colors represent different regional associations: convective (red), equatorial (blue), arid (gold), and mid-latitude (green). The joints with respect to Heat Index are: a) *T*, b) *RH*, c) T_w, d) *THIC*, e) Θ_E, and f) *Q*.

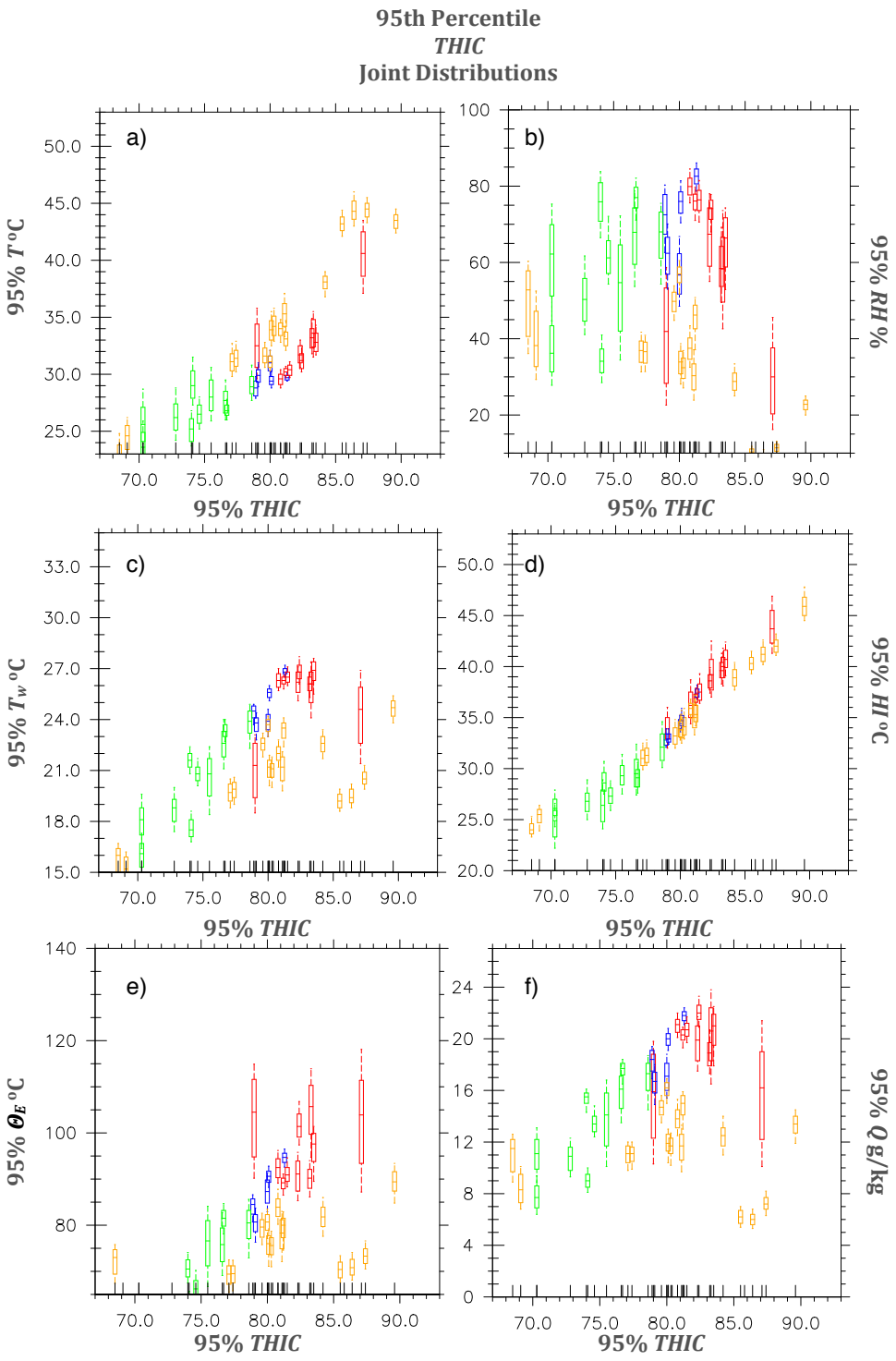

Figure 6: 95th percentile joint distribution box and whisker plots of *THIC*. Each box and whisker plot is a metropolitan area location. The colors represent different regional associations: convective (red), equatorial (blue), arid (gold), and mid-latitude (green). The joints with respect to *THIC* are: a) *T*, b) *RH*, c) T_w, d) *HI*, e) Θ_E, and f) *Q*.

5. DISCUSSION

We will discuss the results of the implementation of the HumanIndexMod within CLM4.5 in two segments, one on moist thermodynamical routines and their applications within the global modeling framework. Next we discuss the heat stress indices, and their variability within the CLM4.5 framework.

5.1 Moist Thermodynamics

Moist thermodynamic quantities are difficult to calculate efficiently. Decades of research effort has produced numerous methods to produce fast computations at the expense of accuracy. One of the more commonly used methods has been the use of polynomial fits to Clausius-Clapeyron water vapor calculations (Wexler, 1976; Wexler, 1977; Flatau et al.,1992). Bolton's (1980) calculations were very accurate, yet, still wrestled with efficiency. 30 years have gone by since Bolton's calculations, and 20 years have passed since Flatau's polynomial fits. Computers have advanced in computational capabilities by orders of magnitude, and with Davies-Jones's (2008) efficient wet bulb calculations, there is a case for updating moist thermodynamical code within Earth system models. CAM5.3 and CLM4.5, the latest versions of core models within CESM1.2 released in June of 2013, still use Flatau's polynomial fits. Our heat stress module has

been accepted into the developer code of CLM4.5 (personal communication with Keith Oleson). With the module in use to calculate heat stress quantities, updating other model code within CESM1.2 will require minimal effort since the code has already been assimilated. An avenue of future work may be spearheading this effort. This will also allow relevant heat stress quantities to be calculated throughout the entire atmospheric model.

Accurate moist thermodynamical calculations, potentially, may point out issues within Earth system models. These are conserved quantities, and unreasonable values bring another diagnostic analysis tool to these GCMs. The soil parameterization issue (see section 4.1) is a possible candidate for further evaluation. Additionally, this issue has been confirmed independently at NCAR (Sean Swenson, personal communication). The maximum ~6 hour period is equivalent to having Θ_E temperatures at hurricane levels (Smith and Montgomery, 2012)–in the middle of a desert. The biases in the African and Arabian monsoons has been a systematic issue within the history of CAM (Meehl et al., 2006; Cook et al., 2012), and linking the monsoon dynamics back to thermodynamics may help explain this issue.

5.2 Heat Stress Indices

Heat stress indices are a measurement of thermal load on humans, as well as describe the covariance of temperature and humidity. By characterizing the extremes in climate models, we can make predictions about both variability of extremes and limits to human adaptability.

The spatial plots of heat stress, and the variables that are used to calculate those indices, show a consistent pattern of how extremes are organized within the physical system. The heat stress indices also describe two different regimes within the climate system. There is the arid regime, and non-arid regime. Heat stress indices respond directly to high *T* variations with a inversely varying *RH* (Figure 5a,b and 6a,b; gold). The *T* response is robust and is in previous versions of CLM (Oleson et al., 2011; Fischer et al., 2012; Oleson et al., 2013). The maximum *T* is the driver for maximum T_w in arid regions (Figure 1j). The *T* and heat stress spatial patterns are similar over arid regions (Figure 1b, 1f). *T* is the driver of heat stress in the arid regions. Atmospheric stability may explain why *T* is the driving mechanism. The arid regions are areas of subsidence in overall general circulation. Areas of subsidence have low specific humidity values, even at the extreme T_w values (Figure 1l).

The rest of the world is non-arid in heat stress, however, there are residual patterns. Equatorial regions (Figures 3-6; blue) have a nearly invariable heat stress state. Solar insolation is nearly constant on yearly timescales, and implies that small changes in mean global temperature will cause major shifts in amount of heat stress within these zones. Past modeling studies have demonstrated that urban equatorial regions transition to a nearly permanent high heat stress environment when considering global warming (Fischer et al., 2012; Oleson et al., 2013). The convective regions (Figures 3-6; red) are areas with strong heat stress maximums and are often coastal locations. Many of these metropolitan areas are in monsoonal regions, which both have strong yearly variability and seasonal changes in insolation, and is reflected in the variability as

compared to equatorial zones (Figures 5f and 6f). Heat stress in these zones is expected to increase dramatically when considering global warming (Fischer and Knutti, 2012; Dunne et al., 2013; Oleson et al., 2013). Outside of the arid regions, the convective zones have the highest annual heat stress (Figures 1a, 1e, 1f, 5, and 6). For the equatorial zones, there is a near constant state of high moisture and temperature. Even with convection, the T_w remains constant, due to a 'constant' energy source (the Sun), and replacement of water loss by advection. The convective zones, during their respective summer conditions, are also near a constant state of high moisture and temperature. Again, the source of energy from the Sun and replacement of water through advection.

The last regional area is the mid-latitudes. Like the equatorial and convective areas, the heat stress in mid-latitude zones is governed by moist thermodynamics in summer (Figures 4a, 4e, 5c, 5e, 6c, and 6e; green). The difference between arid regions and the rest of the world imply that two types of heat stress metrics may be considered. In the arid regions, moist thermodynamic quantities diverge from heat stress metrics, and metrics that include heat load may be necessary for quantifying heat stress (e.g. Oleson et al., 2013 and comparisons between Phoenix and Houston). For the non-arid regions, moist thermodynamic quantities produce the same results as heat stress metrics.

6. BROADER IMPACTS

We presented the new HumanIndexMod that calculates numerous atmospheric variable dependent heat stress metrics and an accurate water vapor calculation. The heat stress metrics cover the three development philosophies: comfort, physiological, and empirically based algorithms. The code is designed, with minimal effort, to be implemented into general circulation and weather forecasting models. Additionally, this code is intended to be used with archived data formats.

Furthermore, we have presented HumanIndexMod results from the latest public release version of CLM4.5 (CESM1.2). Demonstrating the versatility of the HumanIndexMod within CLM4.5, we have located a possible avenue for model improvement, the desert sand parameterizations. We also show that the module may be used to explore a new avenue of research in human heat stress through systematic evaluation and comparison of different heat stress metrics. Our results show that moist thermodynamic quantities (T_w, T_E, etc.) produce lower values of the magnitude of heat stress in arid environments as compared to comfort based algorithms (*HI*, *AT*, *HUMIDEX*, etc.).

Our approach has limitations. None of the metrics in the HumanIndexMod include the effects of solar and thermal radiation. Radiation is a non-negligible

component of heat stress. As a consequence, the heat stress metrics presented always assume that the subject is not in direct solar exposure. Additionally, the indices represent a diagnostic environment for heat stress. These metrics do not incorporate a prognostic component of the human thermal system. Heat storage is assumed to be zero. As a consequence, it is difficult to determine the direct impacts of prolonged/repeat exposure from heat stress, only empirically derived impacts. Lastly, the simulations we show only characterize the modern climate system in broad strokes. Further analysis of specific heat stress events (2003 European Heat wave, 2010 Russian Heat wave, or prolonged exposure to heat in Nicaragua, etc.), is required to analyze each metric and recommend an appropriate heat algorithm for future policymaking. Climate change simulations and assessments are not performed, and this work does not characterize possible future scenarios. Additionally, the simulation in this thesis is only one realization of the many reanalysis products available.

Overall, the HumanIndexMod provide a systematic way for implementing an aspect of thermo-animal physiology into the global climate modeling framework. Incorporating the HumanIndexMod into a variety of different models would provide a baseline for model-model comparisons of heat stress, such as the Coupled Model Intercomparison Project (CMIP) and other collaborative modeling frameworks. We encourage researchers to incorporate the HumanIndexMod within their research environments.

LIST OF REFERENCES

LIST OF REFERENCES

Australian Bureau of Meteorology: About the WBGT and Apparent Temperature indices–Australian Bureau of Meteorology. http://www.bom.gov.au/info/thermal_stress/.

American College of Sports Medicine. (1984). Position stand on the prevention of thermal injuries during distance running. *Medical Journal of Australia*, 141, 876–879.

American College of Sports Medicine. (1987). Position stand on the prevention of thermal injuries during distance running. *Medicine and Science in Sports and Exercise*, *19*(5), 529-533.

Alfano, F. R. D. A., Palella, B. I., & Riccio, G. (2012). On the Problems Related to Natural Wet Bulb Temperature Indirect Evaluation for the Assessment of Hot Thermal Environments by Means of WBGT. *Annals of occupational hygiene*, *56*(9), 1063-1079.

Baker, L. A., Brazel, A. J., Selover, N., Martin, C., McIntyre, N., Steiner, F. R., Nelson, A., & Musacchio, L. (2002). Urbanization and warming of Phoenix (Arizona, USA): Impacts, feedbacks and mitigation. *Urban Ecosystems*, *6*(3), 183-203.

Belding, H. S., & Hatch, T. F. (1955). Index for evaluating heat stress in terms of resulting physiological strain. *Heating, piping and air conditioning*, *27*(8), 129.

Beniston, M. (2004). The 2003 heat wave in Europe: A shape of things to come? An analysis based on Swiss climatological data and model simulations. *Geophysical Research Letters*, *31*(2).

Berglund, L. G., & Yokota, M. (2005). *Comparison of human responses to prototype and standard uniforms using three different human simulation models: HSDA, Scenario_J and Simulink2NM* (No. USARIEM-T05-08). ARMY RESEARCH INST OF ENVIRONMENTAL MEDICINE NATICK MA BIOPHYSICS AND BIOMEDICAL MODELING DIV.

Berrisford, P., Kållberg, P., Kobayashi, S., Dee, D., Uppala, S., Simmons, A. J., Poli, P., & Sato, H. (2011). Atmospheric conservation properties in ERA-Interim. *Quarterly Journal of the Royal Meteorological Society*, *137*(659), 1381-1399.

Betts, A. K., & Dugan, F. J. (1973). Empirical formula for saturation pseudoadiabats and saturation equivalent potential temperature. *Journal of Applied Meteorology*, *12*(4), 731-732.

Bolton, D. (1980). The computation of equivalent potential temperature. *Monthly weather review*, *108*(7), 1046-1053.

Bonan, G. B., Levis, S., Kergoat, L., & Oleson, K. W. (2002). Landscapes as patches of plant functional types: An integrating concept for climate and ecosystem models. *Global Biogeochemical Cycles*, *16*(2), 1021.

Bouchama, A., Al Mohanna, F., El-Sayed, R., Eldali, A., Saussereau, E., Chollet-Martin, S., Olliver, V., de Prost, D., & Roberts, G. (2005). Experimental heatstroke in baboon: analysis of the systemic inflammatory response. *Shock*, *24*(4), 332-335.

Brake, D. J. (2001). Calculation of the natural (unventilated) wet bulb temperature, psychrometric dry bulb temperature and wet bulb globe temperature from standard psychrometric measurements. *J Mine Vent Soc S Afr*, *54*(108), 12.

Breckenridge, J. R., & Goldman, R. F. (1971). Solar heat load in man. *Journal of Applied Physiology*, *31*(5), 659-663.

Bröde, P., Krüger, E. L., Rossi, F. A., & Fiala, D. (2012). Predicting urban outdoor thermal comfort by the Universal Thermal Climate Index UTCI—a case study in Southern Brazil. *International journal of biometeorology*, *56*(3), 471-480.

Budd, G. M. (2008). Wet-bulb globe temperature (WBGT)—its history and its limitations. *Journal of Science and Medicine in Sport*, *11*(1), 20-32.

Buffenstein, R., & Yahav, S. (1991). Is the naked mole-rat *Hererocephalus glaber* an endothermic yet poikilothermic mammal?. *Journal of Thermal Biology*, *16*(4), 227-232.

Buller, M. J., Tharion, W. J., Hoyt, R. W., & Jenkins, O. C. (2010, May). Estimation of Human Internal Temperature from Wearable Physiological Sensors. In *IAAI*.

Bynum, G. D., Pandolf, K. B., Schuette, W. H., Goldman, R. F., Lees, D. E., Whang-Peng, Atkinson, E. R., & Bull, J. M. (1978). Induced hyperthermia in sedated humans and the concept of critical thermal maximum. *American Journal of Physiology-Regulatory, Integrative and Comparative Physiology*, *235*(5), R228-R236.

Byrne, C., Lee, J. K. W., Chew, S. A. N., Lim, C. L., & Tan, E. Y. M. (2006). Continuous thermoregulatory responses to mass-participation distance running in heat. *Medicine and science in sports and exercise*, *38*(5), 803.

Cain, B. (2006). *A preliminary study of heat strain using modelling and simulation* (No. DRDC-TR-2005-255). Defense Research and Development Toronto (Canada).

Casado, M., Ortega, P., Masson-Delmotte, V., Risi, C., Swingedouw, D., Daux, V., Genty, D., Maignam, F. Solomina, O., Vinther, B., Viovy, N., & Yiou, P. (2013). Impact of precipitation intermittency on NAO-temperature signals in proxy records. *Climate of the Past*, *9*(2), 871-886.

Chan, A. P., Yam, M. C., Chung, J. W., & Yi, W. (2012). Developing a heat stress model for construction workers. *Journal of Facilities Management*, *10*(1), 59-74.

Conti, S., Meli, P., Minelli, G., Solimini, R., Toccaceli, V., Vichi, M., Beltrano, C., & Perini, L. (2005). Epidemiologic study of mortality during the Summer 2003 heat wave in Italy. *Environmental research*, *98*(3), 390-399.

Cook, K. H., Meehl, G. A., & Arblaster, J. M. (2012). Monsoon regimes and processes in CCSM4. Part II: African and American monsoon systems. *Journal of Climate*, *25*(8), 2609-2621.

Cortez, O. D. (2009). Heat stress assessment among workers in a Nicaraguan sugarcane farm. *Global Health Action*, *2*.

Crowe, J., de Joode, B. V. W., & Wesseling, C. (2009). A pilot field evaluation on heat stress in sugarcane workers in Costa Rica: What to do next?. *Global Health Action*, *2*.

Crowe, J., Moya-Bonilla, J. M., Román-Solano, B., & Robles-Ramírez, A. (2010). Heat exposure in sugarcane workers in Costa Rica during the non-harvest season. *Global Health Action*, *3*.

Davies-Jones, R. (2008). An efficient and accurate method for computing the wet-bulb temperature along pseudoadiabats. *Monthly Weather Review*, *136*(7), 2764-2785.

Davies-Jones, R. (2009). On formulas for equivalent potential temperature. *Monthly Weather Review*, *137*(9), 3137-3148.

Dawson, T. J., & Hulbert, A. J. (1970). Standard metabolism, body temperature, and surface areas of Australian marsupials. *American journal of physiology*, *218*, 1233-1238.

Dee, D. P., Uppala, S. M., Simmons, A. J., Berrisford, P., Poli, P., Kobayashi, S., Andrae, U., Balmaseda, M. A., Balsamo, G., Bauer, P., Bechtold, P., Beljaars, A. C. M., van de Berg, L., Bidot, J., Bormann, N., Delsol, C., Dragani, R., Fuentes, M., Geer, A. J., Haimberger, L., Healy, S. B., Hersbach, H., Holm, E. V., Isaken, L., Kallberg, P., Kohler, M., Matricardi, M., McNally, A. P., Monge-Sanz, B. M., Morcrette, J.-J., Park, B.-K., Peubey, C., de Rosnay, P., Tavolato, C., Thepaut, J.-N., & Vitart, F. (2011). The ERA-Interim reanalysis: Configuration and performance of the data assimilation system. *Quarterly Journal of the Royal Meteorological Society*, *137*(656), 553-597.

Diffenbaugh, N. S., Pal, J. S., Giorgi, F., & Gao, X. (2007). Heat stress intensification in the Mediterranean climate change hotspot. *Geophysical Research Letters*, *34*(11).

Department of Health and Human Services, (DHHS), National Institute for Occupational Safety and Health (NIOSH): Criteria for a Recommended Standard — Occupational Exposure to Hot Environments (DHHS/NIOSH Pub. No. 86-113). Washington, D.C.: DHHS, NIOSH, 1986.

Dole, R., Hoerling, M., Perlwitz, J., Eischeid, J., Pegion, P., Zhang, T., Quan, X.-W., Xu, T., & Murray, D. (2011). Was there a basis for anticipating the 2010 Russian heat wave?. *Geophysical Research Letters*, *38*(6).

Dunne, J. P., John, J. G., Shevliakova, E., Stouffer, R. J., Krasting, J. P., Malyshev, S. L., Milly, P. C. D., Sentman, L. T., Adcroft, A. J., Cooke, W., Dunne, K. A., Griffies, S. M., Hallberg, R. W., Harrison, M. J., Levy, H., Wittenberg, A. T., Phillips, P. J., & Zadeh, N. (2013). GFDL's ESM2 Global Coupled Climate–Carbon Earth System Models. Part II: Carbon System Formulation and Baseline Simulation Characteristics. *Journal of Climate*, *26*(7), 2247-2267.

Dunne, J. P., Stouffer, R. J., & John, J. G. (2013). Reductions in labour capacity from heat stress under climate warming. *Nature Climate Change*.

Epstein, Y., & Moran, D. S. (2006). Thermal comfort and the heat stress indices. *Industrial Health*, *44*(3), 388-398.

Fanger, P. O. (1970). Thermal comfort. Analysis and applications in environmental engineering. *Thermal comfort. Analysis and applications in environmental engineering.*

Fiala, D., Lomas, K. J., & Stohrer, M. (1999). A computer model of human thermoregulation for a wide range of environmental conditions: the passive system. *Journal of Applied Physiology*, *87*(5), 1957-1972.

Fiala, D., Lomas, K. J., & Stohrer, M. (2001). Computer prediction of human thermoregulatory and temperature responses to a wide range of environmental conditions. *International Journal of Biometeorology*, *45*(3), 143-159.

Fischer, E. M., Oleson, K. W., & Lawrence, D. M. (2012). Contrasting urban and rural heat stress responses to climate change. *Geophysical research letters*, *39*(3).

Fischer, E. M., & Knutti, R. (2012). Robust projections of combined humidity and temperature extremes. *Nature Climate Change*.

Flatau, P. J., Walko, R. L., & Cotton, W. R. (1992). Polynomial fits to saturation vapor pressure. *Journal of Applied Meteorology*, *31*, 1507-1507.

Gagge, A. P. (1971). An effective temperature scale based on a simple model of human physiological regulatory response. *ASHRAE Trans.*, *77*, 247-262.

Gardner, J. W., Kark, J. A., Karnei, K., Sanborn, J. S., Gastaldo, E. D. W. A. R. D., Burr, P. E. G. G. Y., & Wenger, C. B. (1996). Risk factors predicting exertional heat illness in male Marine Corps recruits. *Medicine and science in sports and exercise*, *28*(8), 939-944.

Gates, R. S., Timmons, M. B., & Bottcher, R. W. (1991). Numerical optimization of evaporative misting systems. *Transactions of the ASAE*, *34*.

Gates, R. S., Usry, J. L., Nienaber, J. A., Turner, L. W., & Bridges, T. C. (1991). An optimal misting method for cooling livestock housing. *Transactions of the ASAE*, *34*.

Gaughan, J., Lacetera, N., Valtorta, S. E., Khalifa, H. H., Hahn, L., & Mader, T. (2009). Response of domestic animals to climate challenges. In *Biometeorology for Adaptation to Climate Variability and Change* (pp. 131-170). Springer Netherlands.

Gent, P. R., Danabasoglu, G., Donner, L. J., Holland, M. M., Hunke, E. C., Jayne, S. R., Lawrence , D. M., Neale, R. B., Rasch, P. J., Vertenstein, M., Worley, P. H., Yang, Z.-L., & Zhang, M. (2011). The community climate system model version 4. *Journal of Climate*, *24*(19), 4973-4991.

Gonzalez, R. R., Berglund, L. G., & Stolwijk, J. A. J. (1980). Thermoregulation in humans of different ages during thermal transients. In *Proceedings of the Satellite of 28th International Congress of Physiological Sciences. Pecs, Hungary: Pergamon* (pp. 357-361).

Gonzalez, R. R. (2004). *SCENARIO* revisited: comparisons of operational and rational models in predicting human responses to the environment. *Journal of Thermal Biology*, *29*(7), 515-527.

Gonzalez, R. R., Cheuvront, S. N., Ely, B. R., Moran, D. S., Hadid, A., Endrusick, T. L., & Sawka, M. N. (2012). Sweat rate prediction equations for outdoor exercise with transient solar radiation. *Journal of Applied Physiology*, *112*(8), 1300-1310.

Gribok, A. V., Buller, M. J., & Reifman, J. (2008). Individualized short-term core temperature prediction in humans using biomathematical models. *Biomedical Engineering, IEEE Transactions on*, *55*(5), 1477-1487.

Havenith, G., Fiala, D., Błazejczyk, K., Richards, M., Bröde, P., Holmér, I., Rintamaki, H., Benshabat, Y., & Jendritzky, G. (2012). The UTCI-clothing model. *International journal of biometeorology*, *56*(3), 461-470.

Hightower, L. E., & Guidon, P. T. (1989). Selective release from cultured mammalian cells of heat-shock (stress) proteins that resemble glia-axon transfer proteins. *Journal of cellular physiology*, *138*(2), 257-266.

Hyatt, O. M., Lemke, B., & Kjellstrom, T. (2010). Regional maps of occupational heat exposure: past, present, and potential future. *Global health action*, *3*.

Ingram, D. L. (1965). Evaporative cooling in the pig. *Nature*, (207), 415-416.

IPCC. (2012). Summary for Policymakers. In: Managing the Risks of Extreme Events and Disasters to Advance Climate Change Adaptation. [Field, C.B., V. Barros, T.F. Stocker, D. Qin, D.J. Dokken, K.L. Ebi, M.D. Mastrandrea, K.J. Mach, G.-K. Plattner, S.K. Allen, M. Tignor, and P.M. Midgley (eds.)]. A Special Report of Working Groups I and II of the Intergovernmental Panel on Climate Change. Cambridge University Press, Cambridge, UK, and New York, NY, USA, 1-19.

Jendritzky, G., & Tinz, B. (2009). The thermal environment of the human being on the global scale. *Global Health Action*, *2*.

Jendritzky, G., Havenith, G., Weihs, P., & Batchvarova, E. (2009). Towards a Universal Thermal Climate Index UTCI for assessing the thermal environment of the human being. *Final Report COST Action*, *730*.

Kalkstein, L. S., & Greene, J. S. (1997). An evaluation of climate/mortality relationships in large US cities and the possible impacts of a climate change. *Environmental health perspectives*, *105*(1), 84.

Kalnay, E., Kanamitsu, M., Kistler, R., Collins, W., Deaven, D., Gandin, L., Iredell, M., Saha, S., White, G., Woollen, J., Zhu, Y., Chelliah, M., Ebisuzaki, W., Higgins, W., Janowiak, J., Mo, K. C., Ropelewski, C., Wang, J., Leetmaa, A., Reynolds, R., Jenne, R., & Joseph, D. (1996). The NCEP/NCAR 40-year reanalysis project. *Bulletin of the American meteorological Society*, *77*(3), 437-471.

Kanamitsu, M., Ebisuzaki, W., Woollen, J., Yang, S. K., Hnilo, J. J., Fiorino, M., & Potter, G. L. (2002). Ncep-doe amip-ii reanalysis (r-2). *Bulletin of the American Meteorological Society*, *83*(11), 1631-1643.

Khan, Z. A., Maniyan, S., Mokhtar, M., Quadir, G. A., & Seetharamu, K. N. (2004). A Generalised Transient Thermal Model for Human Body. *Jurnal Mekanikal*, (18), 78-97.

Kjellstrom, T., Kovats, R. S., Lloyd, S. J., Holt, T., & Tol, R. S. (2009). The direct impact of climate change on regional labor productivity. *Archives of Environmental & Occupational Health*, *64*(4), 217-227.

Koca, R. W., Hughes, W. C., & Christianson, L. L. (1991). Evaporative cooling pads: test procedure and evaluation. *Applied Engineering in Agriculture*, *7*.

Koppe, C., Kovats, S., Jendritzky, G., & Menne, B. (2004). Heat-waves: risks and responses. Health and Global Environmental Change SERIES, No. 2. *World Health Organization*.

Kraning, K. K., & Gonzalez, R. R. (1991). Physiological consequences of intermittent exercise during compensable and uncompensable heat stress. *Journal of Applied Physiology*, *71*(6), 2138-2145.

Kraning, K. K., & Gonzalez, R. R. (1997). A mechanistic computer simulation of human work in heat that accounts for physical and physiological effects of clothing, aerobic fitness, and progressive dehydration. *Journal of thermal biology*, *22*(4), 331-342.

Keuhn, L. A., Stubbs, R. A., & Weaver, R. S. (1970). *Theory of the Globe Thermometer* (No. DRET-RP-745). Defense Research Establishment Toronto Downsview (Ontario).

Lawrence, M. G. (2005). The relationship between relative humidity and the dewpoint temperature in moist air: A simple conversion and applications. *Bulletin of the American Meteorological Society*, *86*(2), 225-233.

Lawrence, D. M., Oleson, K. W., Flanner, M. G., Thornton, P. E., Swenson, S. C., Lawrence, P. J., Zeng, X., Yang, Z.-L., Levis, S., Sakaguchi, K., Bonan, G. B., & Slater, A. G. (2011). Parameterization improvements and functional and structural advances in version 4 of the Community Land Model. *Journal of Advances in Modeling Earth Systems*, *3*(1).

Li, B., Sain, S., Mearns, L. O., Anderson, H. A., Kovats, S., Ebi, K. L., ... & Patz, J. A. (2012). The impact of extreme heat on morbidity in Milwaukee, Wisconsin. *Climatic change*, *110*(3-4), 959-976.

Liljegren, J. C., Carhart, R. A., Lawday, P., Tschopp, S., & Sharp, R. (2008). Modeling the wet bulb globe temperature using standard meteorological measurements. *Journal of Occupational and Environmental Hygiene*, *5*(10), 645-655.

Lucas, E. M., Randall, J. M., & Meneses, J. F. (2000). Potential for evaporative cooling during heat stress periods in pig production in Portugal (Alentejo). *Journal of Agricultural Engineering Research*, *76*(4), 363-371.

Lupi, O. (2008). Ancient adaptations of human skin: why do we retain sebaceous and apocrine glands?. *International journal of dermatology*, *47*(7), 651-654.

Maloney, S. K., & Forbes, C. F. (2011). What effect will a few degrees of climate change have on human heat balance? Implications for human activity. *International journal of biometeorology*, *55*(2), 147-160.

Masterton, J.M., Richardson, F.A. (1979). Humidex, a method of quantifying human discomfort due to excessive heat and humidity. *Environment Canada, Atmospheric Environment Service, Downsview, Ontario,* CLI 1-79.

Matzarakis, A., & Mayer, H. (1991). The extreme heat wave in Athens in July 1987 from the point of view of human biometeorology. *Atmospheric Environment. Part B. Urban Atmosphere*, *25*(2), 203-211.

Meehl, G. A., Arblaster, J. M., Lawrence, D. M., Seth, A., Schneider, E. K., Kirtman, B. P., & Min, D. (2006). Monsoon regimes in the CCSM3. *Journal of climate*, *19*(11), 2482-2495.

Meinshausen, M., Smith, S. J., Calvin, K., Daniel, J. S., Kainuma, M. L. T., Lamarque, J. F., Matsumoto, K., Montzka, S. A., Raper, S. C. B., Riahi, K., Thomson, A., Velders, G. J. M., & van Vuuren, D. P. P. (2011). The RCP greenhouse gas concentrations and their extensions from 1765 to 2300. *Climatic Change*, *109*(1-2), 213-241.

Minard, D., Belding, H. S., & Kingston, J. R. (1957). Prevention of heat casualties. *Journal of the American Medical Association*, *165*(14), 1813-1818.

Mitchell, D., Maloney, S. K., Jessen, C., Laburn, H. P., Kamerman, P. R., Mitchell, G., & Fuller, A. (2002). Adaptive heterothermy and selective brain cooling in arid-zone mammals. *Comparative Biochemistry and Physiology Part B: Biochemistry and Molecular Biology*, *131*(4), 571-585.

Mitchell, D., Fuller, A., & Maloney, S. K. (2009). Homeothermy and primate bipedalism: Is water shortage or solar radiation the main threat to baboon (*Papio hamadryas*) homeothermy?. *Journal of human evolution*, *56*(5), 439-446.

Mitchell, T. D., & Jones, P. D. (2005). An improved method of constructing a database of monthly climate observations and associated high-resolution grids. *International journal of climatology*, *25*(6), 693-712.

Moran, D. S., Pandolf, K. B., Shapiro, Y., Heled, Y., Shani, Y., Mathew, W. T., & Gonzalez, R. R. (2001). An environmental stress index (ESI) as a substitute for the wet bulb globe temperature (WBGT). *Journal of thermal biology*, *26*(4), 427-431.

National Weather Service. Office of Climate, Water, and Weather Services. (2012) http://www.nws.noaa.gov/os/heat/index.shtml.

Nilsson, M., & Kjellstrom, T. (2010). Climate change impacts on working people: how to develop prevention policies. *Global health action*, *3*.

O'Brien, C., Cadarette, B. S., Endrusick, T. L., Blanchard, L. A., Xu, X., Berglund, L. G., Sawka, M., N., & Hoyt, R. W. (2008). *General Procedure for Protective Cooling and Equipment Evaluations Relative to Heat and Cold Stress* (No. TN08-01). ARMY RESEARCH INST OF ENVIRONMENTAL MEDICINE NATICK MA THERMAL AND MOUNTAIN MEDICINE DIVISION.

Occupational Safety and Health Administration. http://www.osha.gov/oilspills/heatstress.html (2010).

O'Donnell, J. K., Tobey, M., Weiner, D. E., Stevens, L. A., Johnson, S., Stringham, P., Cohen, B., & Brooks, D. R. (2011). Prevalence of and risk factors for chronic kidney disease in rural Nicaragua. *Nephrology Dialysis Transplantation*, *26*(9), 2798-2805.

Oleson, K. W., Niu, G. Y., Yang, Z. L., Lawrence, D. M., Thornton, P. E., Lawrence, P. J., Stockli, R., Dickinson, R. E., Bonan, G. B., Levis, S., Dai, A., & Qian, T. (2008). Improvements to the Community Land Model and their impact on the hydrological cycle. *Journal of Geophysical Research: Biogeosciences (2005–2012)*, *113*(G1).

Oleson, K. W., Bonan, G. B., Feddema, J., Vertenstein, M., & Grimmond, C. S. B. (2008). An urban parameterization for a global climate model. Part I: Formulation and evaluation for two cities. *Journal of Applied Meteorology and Climatology*, *47*(4), 1038-1060.

Oleson, K. W., Bonan, G. B., Feddema, J., & Vertenstein, M. (2008). An urban parameterization for a global climate model. Part II: Sensitivity to input parameters and the simulated urban heat island in offline Simulations. *Journal of Applied Meteorology and Climatology*, *47*(4), 1061-1076.

Oleson, K.W., D.M. Lawrence, G.B. Bonan, M.G. Flanner, E. Kluzek, P.J. Lawrence, S. Levis, S.C. Swenson, P.E. Thornton, A. Dai, M. Decker, R. Dickinson, J. Feddema, C.L. Heald, F. Hoffman, J.-F. Lamarque, N. Mahowald, G.-Y. Niu, T. Qian, J. Randerson, S. Running, K. Sakaguchi, A. Slater, R. Stockli, A. Wang, Z.-L. Yang, Xi. Zeng, and Xu. Zeng, (2010). Technical Description of version 4.0 of the Community Land Model (CLM). NCAR Technical Note NCAR/TN-478+STR, National Center for Atmospheric Research, Boulder, CO, 257 pp.

Oleson, K.W., G.B. Bonan, J. Feddema, M. Vertenstein, and E. Kluzek, 2010: Technical Description of an Urban Parameterization for the Community Land Model (CLMU). NCAR Technical Note NCAR/TN-480+STR, DOI: 10.5065/D6K35RM9.

Oleson, K. W., Bonan, G. B., Feddema, J., & Jackson, T. (2011). An examination of urban heat island characteristics in a global climate model. *International Journal of Climatology*, *31*(12), 1848-1865.

Oleson, K. (2012). Contrasts between urban and rural climate in CCSM4 CMIP5 climate change scenarios. *Journal of Climate*, *25*(5), 1390-1412.

Oleson, K.W., D.M. Lawrence, G.B. Bonan, B. Drewniak, M. Huang, C.D. Koven, S. Levis, F. Li, W.J. Riley, Z.M. Subin, S.C. Swenson, P.E. Thornton, A. Bozbiyik, R. Fisher, E. Kluzek, J.-F. Lamarque, P.J. Lawrence, L.R. Leung, W. Lipscomb, S. Muszala, D.M. Ricciuto, W. Sacks, Y. Sun, J. Tang, Z.-L. Yang, 2013: Technical Description of version 4.5 of the Community Land Model (CLM). Ncar Technical Note NCAR/TN-503+STR, National Center for Atmospheric Research, Boulder, CO, 422 pp, DOI: 10.5065/D6RR1W7M.

Oleson, K. W., Monaghan, A., Wilhelmi, O., Barlage, M., Brunsell, N., Feddema, J., Hu, L., & Steinhoff, D. F. (2013). Interactions between urbanization, heat stress, and climate change. *Climatic Change*, 1-17.

O'Neill, M. S., Zanobetti, A., & Schwartz, J. (2003). Modifiers of the temperature and mortality association in seven US cities. *American Journal of Epidemiology*, *157*(12), 1074-1082.

Pandolf, K. B., & Kamon, E. (1974). Respiratory responses to intermittent and prolonged exercise in a hot-dry environment. *Life Sciences*, *14*(1), 187-198.

Parsons, K. (2006). Heat stress standard ISO 7243 and its global application. *Industrial Health*, *44*(3), 368-379.

Renaudeau, D., Collin, A., Yahav, S., De Basilio, V., Gourdine, J. L., & Collier, R. J. (2011). Adaptation to hot climate and strategies to alleviate heat stress in livestock production. *Oceania*, *5*(16.2), 24-4.

Rothfusz, L. P., & Headquarters, N. S. R. (1990). The heat index equation (or, more than you ever wanted to know about heat index). *Fort Worth, Texas: National Oceanic and Atmospheric Administration, National Weather Service, Office of Meteorology*, 90-23.

Semenza, J. C., Rubin, C. H., Falter, K. H., Selanikio, J. D., Flanders, W. D., Howe, H. L., & Wilhelm, J. L. (1996). Heat-related deaths during the July 1995 heat wave in Chicago. *New England Journal of Medicine*, *335*(2), 84-90.

Skamarock, W. C., & Klemp, J. B. (2008). A time-split nonhydrostatic atmospheric model for weather research and forecasting applications. *Journal of Computational Physics*, *227*(7), 3465-3485.

Sheffield, P. E., Herrera, J. G. R., Lemke, B., Kjellstrom, T., & Romero, L. E. B. (2013). Current and Future Heat Stress in Nicaraguan Work Places under a Changing Climate. *Industrial health*, *51*(1), 123-127.

Sherwood, S. C., & Huber, M. (2010). An adaptability limit to climate change due to heat stress. *Proceedings of the National Academy of Sciences*, *107*(21), 9552-9555.

Simon, H. B. (1993). Hyperthermia. *The New England journal of medicine*, *329*(7), 483-487.

Simpson, R. H. (1978). On the computation of equivalent potential temperature. *Monthly Weather Review*, *106*(1), 124-130.

Smith, R. K., & Montgomery, M. T. (2012). How important is the isothermal expansion effect in elevating equivalent potential temperature in the hurricane inner core?. *Quarterly Journal of the Royal Meteorological Society*.

Solomon, S., Qin, D., Manning, M., Alley, R. B., Berntsen, T., Bindoff, N. L., Chen, Z., Chidthaisong, A., Gregory, J. M., Hegerl, G. C., Heimann, M., Hewitson, B., Hoskins, B. J., Joos, F., Jouzel, J., Kattsov, V., Lohmann, U., Matsuno, T., Molina, M., Nicholls, N., Overpeck, J., Raga, G., Ramaswamy, V., Ren, J., Rusticucci, M., Somerville, R., Stocker, T. F., Whetton, P., Wood, R. A., and Wratt, D.: Contribution of Working Group I to the Fourth Assessment Report of the Intergovernmental Panel on Climate Change - Technical Summary, in Climate Change 2007: The Physical Science Basis., edited by S. Solomon, D. Qin, M. Manning, Z. Chen, M. Marquis, K. Averyt, M. Tignor, and H. L. Miller, Cambridge University Press, Cambridge, United Kingdom and New York, NY, USA, 2007.

Song, X., Zhang, G. J., & Li, J. L. (2012). Evaluation of microphysics parameterization for convective clouds in the NCAR Community Atmosphere Model CAM5. *Journal of Climate*, *25*(24), 8568-8590.

Steadman, R. G. (1979). The assessment of sultriness. Part I: A temperature-humidity index based on human physiology and clothing science. *Journal of Applied Meteorology*, *18*(7), 861-873.

Steadman, R. G. (1979). The Assessment of Sultriness. Part II: Efiects of Wind, Extra Radiation and Barometric Pressure on Apparent Temperature. *Journal of Applied Meteorology*, 18, 874-884.

Steadman, R. G. (1984). A universal scale of apparent temperature. *Journal of Climate and Applied Meteorology*, *23*(12), 1674-1687.

Steadman, R. G. (1994). Norms of apparent temperature in Australia. *Aust. Met. Mag*, *43*, 1-16.

Stull, R. (2011). Wet-bulb temperature from relative humidity and air temperature. *Journal of Applied Meteorology and Climatology*, *50*(11), 2267-2269.

Taylor, K. E., Stouffer, R. J., & Meehl, G. A. (2012). An overview of CMIP5 and the experiment design. *Bulletin of the American Meteorological Society*, *93*(4), 485-498.

Thom, E. C. (1959). The discomfort index. *Weatherwise*, *12*(2), 57-61.

Vaneckova, P., Neville, G., Tippett, V., Aitken, P., FitzGerald, G., & Tong, S. (2011). Do biometeorological indices improve modeling outcomes of heat-related mortality?. *Journal of Applied Meteorology and Climatology*, *50*(6), 1165-1176.

Watts, J. D., & Kalkstein, L. S. (2004). The development of a warm-weather relative stress index for environmental applications. *Journal of Applied Meteorology*, *43*(3), 503-513.

Wexler, A. (1976). Vapor pressure formulation for water in range 0 to 100 Degrees C. A revision. *Journal of Research of the National Bureau of Standards–A. Physics and Chemistry*, *80A(5).*

Wexler, A. (1977). Vapor pressure formulation for ice. *Journal of Research of the National Bureau of Standards–A. Physics and Chemistry*, *81*(1), 5-19.

Wexler. Vapor pressure formulation for ice. Journal of Research of the National Bureau of Standards–A. Physics and Chemistry (1977) vol. 81 (1) pp. 5-19.

Willett, K. M., & Sherwood, S. (2012). Exceedance of heat index thresholds for 15 regions under a warming climate using the wet-bulb globe temperature. *International Journal of Climatology*, *32*(2), 161-177.

Withers, P. C., & Jarvis, J. U. M. (1980). The effect of huddling on thermoregulation and oxygen consumption for the naked mole-rat. *Comparative Biochemistry and Physiology Part A: Physiology*, *66*(2), 215-219.

Yokota, M., Berglund, L. G., Santee, W. R., Buller, M. J., & Hoyt, R. W. (2005). Modeling physiological responses to military scenarios: initial core temperature and downhill work. *Aviation, space, and environmental medicine*, *76*(5), 475-480.

Yokota, M., Berglund, L., Cheuvront, S., Santee, W., Latzka, W., Montain, S., Kolka, M., & Moran, D. (2008). Thermoregulatory model to predict physiological status from ambient environment and heart rate. *Computers in biology and medicine*, *38*(11), 1187-1193.

Yokota, M., Bathalon, G. P., & Berglund, L. G. (2008). Assessment of male anthropometric trends and the effects on simulated heat stress responses. *European journal of applied physiology*, *104*(2), 297-302.

Zhang, D. L., Liu, Y., & Yau, M. K. (2002). A multiscale numerical study of Hurricane Andrew (1992). Part V: Inner-core thermodynamics. *Monthly weather review*, *130*(11), 2745-2763.